Journal of Geophysical Research: Oceans

RESEARCH ARTICLE
10.1029/2017JC013651

In Situ and Satellite Observations of Phytoplankton Size Classes in the Entire Continental Shelf Sea, China

Xuerong Sun[1], Fang Shen[1,2], Dongyan Liu[1], Richard G. J. Bellerby[1,3], Yangyang Liu[1], and Rugang Tang[1]

[1]State Key Laboratory of Estuarine and Coastal Research, East China Normal University, Shanghai, China, [2]Institute of Eco-Chongming (IEC), Shanghai, China, [3]Norwegian Institute for Water Research, Bergen, Norway

Key Points:
- In situ PSCs obtained from HPLC method were investigated in the entire continental shelf sea of China, including the BS, the YS, and the ECS
- An improved algorithm was developed and validated to be applicable in the BS, YS, and the ECS
- Diurnal variations of PSCs were obtained when applying the improved algorithm to GOCI images

Correspondence to:
F. Shen,
fshen@sklec.ecnu.edu.cn

Citation:
Sun, X., Shen, F., Liu, D., Bellerby, R. G. J., Liu, Y., & Tang, R. (2018). In situ and satellite observations of phytoplankton size classes in the entire continental shelf sea, China. *Journal of Geophysical Research: Oceans*, *123*, 3523–3544. https://doi.org/10.1029/2017JC013651

Received 29 NOV 2017
Accepted 12 APR 2018
Accepted article online 19 APR 2018
Published online 18 MAY 2018

Abstract Phytoplankton size classes (PSCs) is of great significance for exploring marine ecological and biogeochemical processes. Remote sensing of PSCs has been successfully applied to open oceans; however, it is still quite limited for optically complex coastal oceans. In this study, the entire continental shelf sea of China including Bohai Sea (BS), Yellow Sea (YS), and East China Sea (ECS) characterized by distinctive turbid waters and impacted by plumes of large world-class river (the Changjiang River) was taken as an example of turbid coastal ocean for remotely sensed spatial-temporal distributions of PSCs. In situ data were collected from cruises during April to June in 2014 and an improved algorithm for PSCs retrieval was proposed. PSCs derived from GOCI (Geostationary Ocean Color Imager) images revealed that microplankton was dominant in the BS, the YS, and the nearshore ECS and nanoplankton distributed widely in the entire study area, while picoplankton mainly distributed in the offshore ECS in April, which was consistent with in situ investigation and related to environmental factors. Validation indicated that the improved algorithm provided a more accurate estimation of PSCs, with the root mean square error (RMSE) between estimated and measured size-fractionated concentrations been 0.774, 0.257, and 0.142 mg m^{-3} for micro, nano, and picoplankton, respectively. Diurnal variations of PSCs were mainly affected by tidal currents and light intensity depending on different water types. These illustrated that remote sensed spatial distributions as well as diurnal variations of PSCs are effective in turbid continental shelf seas of China.

1. Introduction

Phytoplankton are the fundamental component of the marine ecosystem. Complex biophysical controls (e.g., irradiance, temperature, salinity, nutrients, and grazing) and anthropogenic impact (e.g., runoff modification, nutrient fluxes) result in large spatial and temporal variations in phytoplankton biomass, community structure, and functionality (Behrenfeld & Boss, 2014; Cloern, 2001; Geider et al., 1998; Lindemann & John, 2014). According to Sieburth et al. (1978), phytoplankton can be operationally divided into three phytoplankton size classes (i.e., microplankton, >20 μm; nanoplankton, 2–20 μm; picoplankton, <2 μm). Phytoplankton size structure are recognized as prime physiological parameters that can influence many marine ecological and biogeochemical processes (Finkel et al, 2010). For example, physiology of phytoplankton, including metabolic rates, growth rates, nutrient uptake, and sinking rate are influenced by cell size (Geider et al., 1986; Waite et al., 1997). Several researches also suggested that size structure can result in different photosynthetic rates and maximum quantum yields, potentially leading to different carbon fixation attributes (Hirata et al., 2009; Uitz et al., 2008). Phytoplankton cell size also influence the optical properties of the ocean surface via light scattering and absorption (Devred et al., 2006; Yentsch & Phinney, 1989). Furthermore, shifts in PSCs can affect the relationship of phytoplankton grazers, and consequently change the function and structure of marine food webs (Legendre & Rassoulzadegan, 1995). Therefore, size structure of phytoplankton has been widely investigated in its role in primary production, carbon-specific photosynthesis, and export production (Cermeño et al., 2005; Hilligsøe et al., 2011; Teira et al., 2001) and utilized in establishing and improving biogeochemical models in marine system (e.g., Aumont et al., 2003; Ward et al., 2012).

A few tools can help to obtain the PSCs, e.g., microscopy, flow cytometry, size-fractionated filtration (SFF), and high performance liquid chromatography (HPLC), and each method has its own advantages and

disadvantages (IOCCG, 2014, Table 2.3). Results of these approaches usually generate a "static" image, for the given environmental conditions and species distributions. However, oceanic environment and phytoplankton distributions are dynamic in space and time. Remote sensing has been regarded as the most important tool for acquiring the continuous observational data spatially and temporally. Hence, the demand to develop methods for identifying PSCs in ocean using remote sensing is urgent. To estimate size-fractionated chlorophyll-a concentration, statistical links between the total chlorophyll-a concentration and PSCs derived from HPLC should be developed. Vidussi et al. (2001) pioneered this approach by selecting seven diagnostic pigments to obtain the fractions of PSCs in the total chlorophyll concentration. Afterward, constant improvements of relationships between the total chlorophyll-a concentration and PSCs were made, such as determining weighting factors of diagnostic pigments and refining assignments of diagnostic pigments for classifying PSCs (Brewin et al., 2010; Hirata et al., 2011; Uitz et al., 2006). Through satellite images (i.e., SeaWiFs and MODIS), these statistical relationships have been successfully utilized in estimating PSCs in global ocean and different oceanic regions (e.g., Brewin et al., 2010, 2012, 2015; Brotas et al., 2013; Hirata et al., 2011; Lin et al., 2014; Uitz et al., 2006).

As mentioned above, relationships between PSCs and total chlorophyll-a concentration have been widely used in global oceanic waters. However, few relationships were carried out in studies for applying in coastal and estuarine systems, particularly in the region with large river plumes. The BS, the YS, and the ECS make up the largest marginal seas, and host one of the most turbid coastal and shelf seas environments globally, supporting high primary and fishery production. They are strongly impacted by the large Changjiang River plumes and adjoining ocean processes, and hydrodynamic features are predominantly driven by variations in tides, large seasonal climatic, and monsoon changes. Together these drivers result in complicated optical, hydrodynamic, and biogeochemical environments, which have a strong influence on the physiology of phytoplankton, leading to region-specific relationships between chlorophyll-a concentration and PSCs, compared to general oceanic conditions. Several studies in which pigment concentrations or size structures of phytoplankton based on SFF methods have been investigated in the BS, the YS, or the ECS (e.g., Deng et al., 2008; Fu et al., 2009; Huang et al, 2006; Sun et al., 2002, 2012; Zhu et al., 2009). However, to the best of our knowledge, there have not been published documents on the application of remote sensing derived PSCs in the entire continental shelf sea of China.

Therefore, we tried to develop an improved algorithm for the monitoring spatial distribution and diurnal variations of PSCs from remote sensing focusing on the BS, the YS, and the ECS. For this purpose, we presented comprehensive in situ measurements derived from HPLC method, aiming to seek relationships between proportions of PSCs and chlorophyll-a concentration. Based on these, existing models (Brewin et al., 2010; Hirata et al., 2011) in estimating PSCs from satellite images were tested for the applicability in the turbid seas affected by terrestrial inputs, of which three-component model (Brewin et al., 2010) was improved by parameterization and subsequently validated through match-ups. Spatial distributions and diurnal variations of PSCs from GOCI observations were analyzed and major controlling environmental factors were discussed.

2. Data and Method

2.1. In Situ Data

The BS is a shallow semienclosed marginal sea on the northern coast of China, of which the mean water depth is no more than 20 m (Figure 1). The Bohai Strait, which connecting the southern of Liaodong Peninsula and the northern of Shandong Peninsula, is defined as the boundary between the BS and the YS. The YS is surrounded by mainland China and the Korean Peninsula, including the north Yellow Sea (NYS) and the south Yellow Sea (SYS). The depth of YS increases gradually from nearshore area (continental shelf) to offshore area (central YS), approximately from 0–40 m to 60–80 m (Figure 1). To its south is the ECS, which is the one of the largest marginal seas in the world. The depth of ECS is shallow in the northwestern area and deep in the southeastern area, due to the impact of continental shelf. The ECS can be broadly divided into three parts: the continental shelf (0–60 m), the outer continental shelf (60–200 m), and Okinawa Trough (200–2,700 m). To the northwest of Taiwan Island, the depth is less than 200 m and it increases significantly toward southeastern area (Figure 1).

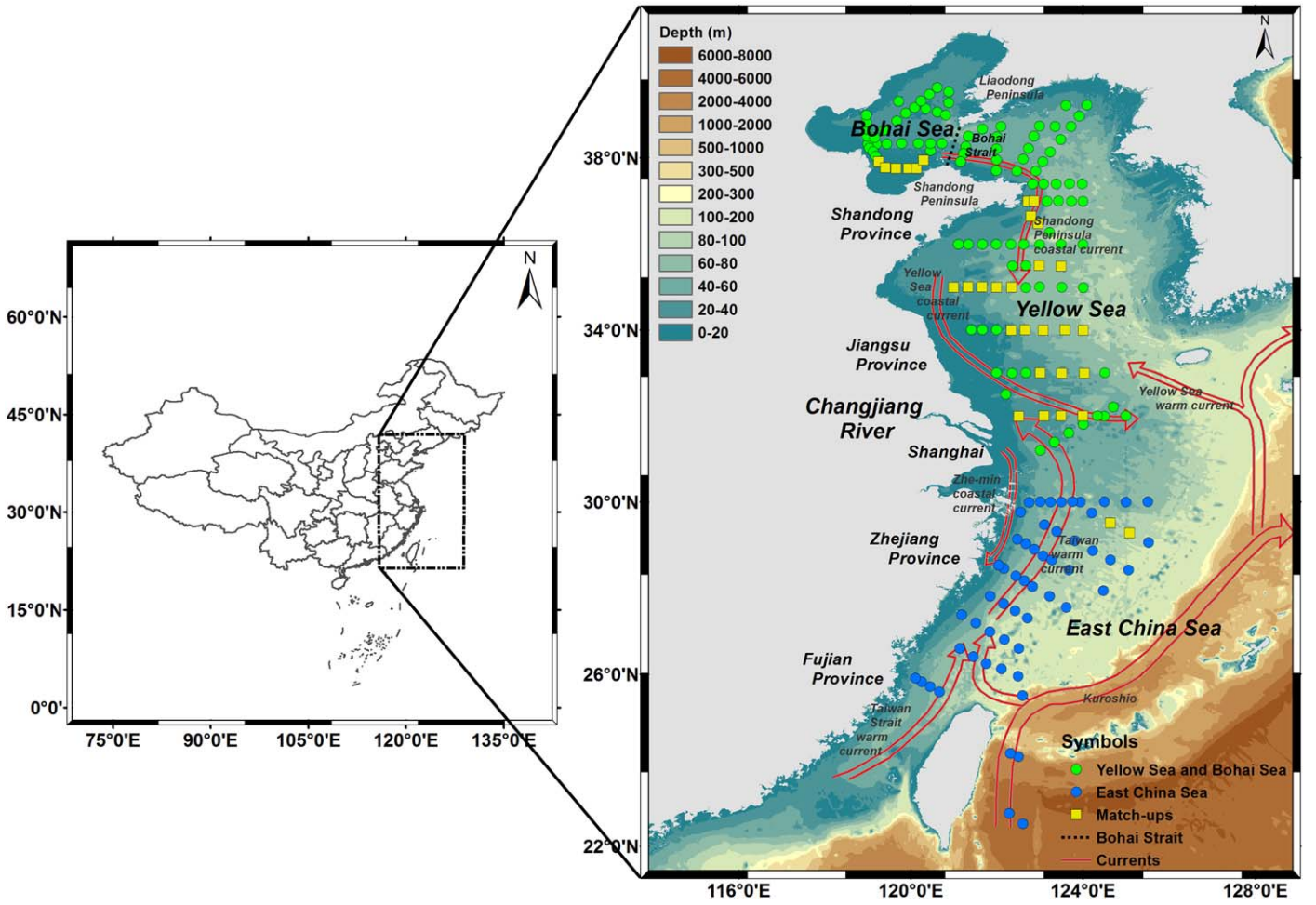

Figure 1. Locations of in situ data used in this study ($N = 180$), circle green symbols represent stations in the Bohai Sea and the Yellow Sea and circle blue ones are the stations in the East China Sea. Square yellow symbols stand for match-ups between in situ measurements and satellite images. Major water masses in summer-half-year are sketched with red lines (after Li et al., 2016). The background seawater depth (The GEBCO_2014 Grid, version 20150318) is obtained from GEBCO (http://www.gebco.net/).

Water masses and current systems are complex in the YS and the ECS during the sampling time, including coastal currents in the east, open ocean water in the west, and mixed water between them (Figure 1). Changjiang River carries large amount of fresh water into the sea, forming Changjiang diluted water (CDW) with low temperature, salinity, and more nutrients. The Shandong Peninsula coastal current comes out of the BS and flows into the YS bypassing the Shandong Peninsula. The Yellow Sea coastal current water flows southward along Jiangsu province and turns southeastward into the ECS, while the Zhe-min coastal current water flows through Zhejiang coastline. By contrast, the Kuroshio water is more powerful and characterized by higher temperature and salinity. After entering the ECS, it flows northeastward along the continental slope. Taiwan Strait warm current flows through Taiwan Strait and moves forward to the north, together with Kuroshio intrusion, forming Taiwan warm current (Chen et al., 1995; Li et al., 2006, 2016; Lie et al., 2001; Quan et al., 2013; Zhang et al., 2008).

The study is based on samples collected on two research cruises in the BS and the YS (31∼40°N, 118∼126°E, 28 April to 18 May) and the ECS (22∼30°N, 121∼126°E, 22 May to 11 June) in 2014 (Figure 1). Water samples for HPLC pigment concentration were collected with Niskin bottles attached to the conductivity-temperature-depth profiler (CTD, Seabird 911) rosette. During the analyses, five outliers of HPLC pigment concentrations were removed and 180 samples were acquired for analyzing surface distributions in the study. Among them, algae bloom was observed at station 4-0-0 (27.76°N, 122.55°E) and quite high chlorophyll concentration was obtained at station H40 (32°N, 124.99°E). To avoid the effect of bloom

Table 1
Symbols and Definitions

Symbol	Description	Units
C_E	The estimation of chlorophyll-a concentration using seven diagnostic pigments (equation (3))	mg m^{-3}
C_{HPLC}	Chlorophyll-a concentration derived from HPLC method (equation (5))	mg m^{-3}
F_m/ F_n/ F_p	Fraction of microplankton/ nanoplankton/ picoplankton (equations (4), (5), and (6))	Dimensionless
C_m/ C_n/ C_p	Concentration of microplankton/ nanoplankton/ picoplankton (equations (9), (10), and (11))	mg m^{-3}
$C_{n,p}$	Concentration of combined of nanoplankton and picoplankton (equation (8))	mg m^{-3}
P_m/ P_n/ P_p	Percentage of microplankton/ nanoplankton/ picoplankton (equations (12), (13), and (14))	%
$C^m_{n,p}$	Asymptotic maximum values for combined nanoplankton and picoplankton (equation (8))	mg m^{-3}
C^m_p	Asymptotic maximum values for picoplankton (equation (10))	mg m^{-3}
$D_{n,p}$	Fraction of total chlorophyll in combined nanoplankton and picoplankton as total chlorophyll tends to zero (equation (8))	Dimensionless
D_p	Fraction of total chlorophyll in picoplankton as total chlorophyll tends to zero (equation (10))	Dimensionless
r	Pearson linear correlation coefficient	Dimensionless
p	p Value	Dimensionless
δ	Bias between concentrations or percentages from measured and estimated data (equation (16))	mg m^{-3} or %
MAE	Mean absolute error between concentrations or percentages from measured and estimated data	mg m^{-3} or %
RMSE	Root mean squared error between concentrations or percentages from measured and estimated data	mg m^{-3} or %
MAE%	Relative mean absolute error between concentrations or percentages from measured and estimated data (equation (17))	%

water on the algorithm (details in section 4.4), these two samples were excluded and 178 samples were left in model reparameterization and validation processes. Underway data such as temperature and salinity were measured by CTD in the BS, the YS, and the ECS as well.

2.2. Satellite Data

The Geostationary Ocean Color Imager (GOCI) is a geostationary-orbiting ocean color sensor with the coverage including the YS and the ECS. The spatial resolution of GOCI image is 500 m and 8 images (one image per hour) are available during daytime (Ryu et al., 2011), not only increasing numbers of image over coastal ocean affected by cloud coverage, but also providing a capability to map short-time scale variation in the entire continental shelf sea of China. In this study, L1B data were obtained from the KOSC (Korea Ocean Satellite Center) website (http://kosc.kiost.ac/eng/). The surface chlorophyll-a concentration products were calculated through the GOCI Data Processing System (GDPS version 1.4.1), in which KOSC standard was the method for atmospheric correction and YOC (Yellow Sea Large Marine Ecosystem Ocean Color Work Group) was the method for chlorophyll-a concentration products. Based on the empirical algorithm applied for coastal waters from Tassan (1994), parameters of the algorithm YOC were optimized for the YS and ECS (Siswanto et al., 2011). The YOC algorithm is:

$$Chla_{yoc} = 10^{\left(0.342 - 2.511 * \log_{10}(R) - 0.277 * \log^2_{10}(R)\right)} \quad (1)$$

$$R = \left(\frac{R_{rs}(443)}{R_{rs}(555)}\right)\left(\frac{R_{rs}(412)}{R_{rs}(490)}\right)^{-1.012} \quad (2)$$

Since a whole GOCI image consists of 4-by-4 subimages taken by one camera, mosaic edge effects of top-of-atmosphere radiance from L1B products at some bands (e.g., Band 1 at 412nm) are the cause of spatial discontinuity of the chlorophyll-a concentration products. Therefore, in this study we utilized neighboring pixel interpolation method to reprocess the neighboring slots in order to avoid discontinuity. After top-of-atmosphere of radiance products which have slot margin effects are exported from the GDPS, pixels values on either sides of the slot margins are extracted to establish linear regression equations and calculate

Table 2
Major Diagnostic Pigments Used for Classification of PSCs From Brewin et al. (2010)*,* Hirata et al. (2011)*, and This Study, Along With the Taxonomic or Biogeochemical Significance (*Ras et al., 2007*)*

Diagnostic pigments	Designation	Brewin et al. (2010)	Hirata et al. (2011)	In this study
Fucoxanthin (Fuco)	Diatoms	Micro	Micro/Nano	Micro
Peridinin (Per)	Dinoflagellates	Micro	Micro	Micro
Alloxanthin (All)	Cryptophytes	Nano	Nano	Nano
19′-but-fucoxanthin (But)	Pelagophytes	Nano	Nano	Nano
19′- hex-fucoxanthin (Hex)	Prymnesiophytes	Nano/Pico	Nano/Pico	Nano/Pico
Chlorophyll-b (Chl-*b*)	Chlorophytes	Pico	Nano	Nano
Divinyl chlorohphyll-b	Prochlorophytes	Pico		
Zeaxanthin (Zea)	Cyanobacteria Prochlorophytes	Pico	Pico	Pico

slopes. Through the judgment of chlorophyll-a concentration, slots with outliers are calculated based on slopes. Then without mosaic edge effects, the processed top-of-atmosphere radiance L1B products are imported to the GOCI images.

Considering the frequency of the GOCI no-cloud overpassing and in situ survey time, the time window of match-ups was set to $\pm$3.5 h. Under the condition of picking images with the shortest time interval, 31 sampling sites were matched to GOCI data in the study area (Figure 1). The matched images were acquired on 30 April, 1 May, 2 May, 3 May, 6 May, 9 May, 12 May, and on 9 June. Average values of 3-by-3 pixel box from the GOCI chlorophyll-a concentration products were regarded as the matched data. Eight images on 7 April 2013 were provided to show the GOCI-derived PSCs and the diurnal variation.

For comparison with physical variables on 7 April 2013, SNPP VIIRS (Suomi NPP Visible Infrared Imaging Radiometer Suite) daily composite sea surface temperature data at 4 km resolution was obtained from OceanColor website (https://oceancolor.gsfc.nasa.gov/).

2.3. Laboratorial Determination of Phytoplankton Size Classes

Laboratorial determination of PSCs was based on the high performance liquid chromatography (HPLC) method. Water samples (100$\sim$2,000 mL) from Niskin bottles were filtered through the Whatman GF/F Glass Microfiber Filters (pore size 0.7 μm, diameter 25 mm), and the filters were kept in the aluminum foil and frozen in liquid nitrogen. Using a Shimadzu LC-20A high-performance liquid chromatography system (Kyoto, Japan), pigment concentrations in the ECS were processed using the method described by Wang et al. (2016). Detailed instrumentation and methodology of samples processing for HPLC pigments in the BS and the YS can be found in Zhang et al., (2016). Twenty phytoplankton pigments were measured, including chlorophyll-c3, chlorophyllide-a, chlorophyll-c2, peridinin, 19-but-fucoxanthin, fucoxanthin, neoxanthin, prasinoxanthin, 19-hex-fucoxanthin, violaxanthin, diadinoxanthin, alloxathin, diatoxanthin, zeaxanthin, lutein, chlorophyll-b, DV-chlorophyll-a, chlorophyll-a, α-carotene, and β-carotene. Pigments or pigment groups can be assigned to individual phytoplankton species, thus characterizing PSCs indirectly. We utilized seven diagnostic pigments (i.e., fucoxanthin, peridinin, alloxanthin, 19-but-fucoxanthin, 19-hex-fucoxanthin, chlorophyll-b and zeaxanthin) considering the differences in phytoplankton species of each study area (Brewin et al., 2010; Hirata et al., 2011) (Table 2).

In the global marine system, Devred et al. (2011) and Hirata et al. (2011) assigned part of the pigment fucoxanthin to the nanoplankton group by involving pigments 19′-but-fucoxanthin and 19′- hex-fucoxanthin in fucoxanthin adjustment when chlorophyll-a concentration was low (0.25 mg m^{-3}), because fucoxanthin

Table 3
Retrieved Parameter Values Derived From Fitting the Three-Component Model to In Situ Pigment Data From the YS and the ECS

Study	$C^m_{n,p}$	$D_{n,p}$	C^m_p	D_p	MAE[a]	MAE[b]
This study	0.329	1.000	0.052	0.914	0.127	0.045

[a]MAE was the mean absolute error between in situ and modeled $C_{n,p}$. [b]MAE was the mean absolute error between in situ and modeled C_p.

was also present in prymnesiophytes and chrysophytes. Considering most water samples were higher than 0.25 mg m^{-3} and diatoms had absolute advantage in the climatic spring in the BS, the YS, and the ECS (Gao et al., 2003; Guo et al., 2014), we assumed that fucoxanthin was a representative for microplankton. Brewin et al. (2010) combined pigments chlorophyll-b and divinyl chlorophyll-b as a whole and treated them as the diagnostic pigments of picoplankton. However, chlorophytes were one of the major composition of nanoplankton in the study area (Gao et al., 2013; Song et al., 2017). Therefore, in this study, chlorophyll-b was regarded as a biomarker of nanoplankton which has been utilized by Hirata et al. (2011). Zeaxanthin and alloxanthin were much lower in the study area, comparing to the other five diagnostic pigments. Even though values were small, these two pigments were detected in most stations through a more sensitive method developed for the purpose of decreasing the detection limit (Zhang et al., 2016).

The estimation of chlorophyll-a concentration (C_E) as proposed by Vidussi et al. (2001) and later refined by Uitz et al. (2006) can be inferred as

$$C_E = 1.41Fuco + 1.41Per + 1.27Hex + 0.6All + 0.35But + 1.01Chl-b + 0.86Zea \tag{3}$$

According to Brewin et al. (2010) and Hirata et al. (2011), the fractions (F) of the size-fractionated chlorophyll-a concentrations can be estimated as

$$F_m = \frac{1.41 \cdot (Fuco + Per)}{C_E} \tag{4}$$

$$F_n = \begin{cases} \dfrac{12.5 \cdot C_{HPLC} \cdot 1.27 \cdot Hex + 1.01 \cdot Chl-b + 0.35 \cdot But + 0.6 \cdot All}{C_E} & , C_{HPLC} < 0.08 mg/m^3 \\ \dfrac{1.27 \cdot Hex + 1.01 \cdot Chl-b + 0.35 \cdot But + 0.6 \cdot All}{C_E} & , C_{HPLC} > 0.08 mg/m^3 \end{cases} \tag{5}$$

and

$$F_p = \begin{cases} \dfrac{(-12.5 \cdot C_{HPLC} + 1) \cdot 1.27 \cdot Hex + 0.86 \cdot Zea}{C_E} & , C_{HPLC} < 0.08 mg/m^3 \\ \dfrac{0.86 \cdot Zea}{C_E} & , C_{HPLC} > 0.08 mg/m^3 \end{cases} \tag{6}$$

The subscripts m, n, and p refer to micro, nano, and picoplankton, respectively. C_{HPLC} represents chlorophyll-a concentration derived from in situ HPLC pigment data. C_{HPLC} and C_E were in good agreement, with a correlation coefficient of 0.843 and p-value of < 0.001. Size-fractionated percentages could be calculated by multiplying fractions by 100, and size-fractionated concentrations could be calculated by multiplying fractions by the C_{HPLC}.

2.4. Estimation of Phytoplankton Size Classes

2.4.1. Three-Component Model of PSCs

Brewin et al. (2010) developed a group of equations based on an underlying conceptual model (Sathyendranath et al., 2001) that was used to quantify the relationship between chlorophyll-a concentration and fractional contribution to chlorophyll-a for each size class. These equations were extended by Brewin et al., (2014, 2015), where total and size-fractionated concentrations are obtained from

$$C_{HPLC} = C_m + C_n + C_p \tag{7}$$

$$C_{n,p} = C_{n,p}^m \left[1 - \exp\left(-\frac{D_{n,p}}{C_{n,p}^m} C_{HPLC} \right) \right] \tag{8}$$

$$C_m = C_{HPLC} - C_{n,p}, \tag{9}$$

$$C_p = C_p^m \left[1 - \exp\left(-\frac{D_p}{C_p^m} C_{HPLC} \right) \right] \tag{10}$$

and

$$C_n = C_{n,p} - C_p \tag{11}$$

where C_{HPLC} is the sum of micro (C_m), nano (C_n), and picoplankton (C_p) chlorophyll-a concentration, and $C_{n,p}$ is the sum of nano and picoplankton. $C_{n,p}^m$ and C_p^m are the asymptotic maximum values for the classes whose sizes are smaller than 20 and 2 μm, respectively. Similarly, $D_{n,p}$ and D_p represent size-fractionated chlorophyll-a concentrations as total chlorophyll-a concentrations tends to zero. Therefore, $D_{n,p}$ and D_p are constrained to be less than or equal to one. The percentage of each PSCs (P_m, P_n, P_p, and $P_{n,p}$) to the C_{HPLC} can be calculated by dividing the size-fractionated chlorophyll-a concentration by the total and multiplying by 100, which are

$$P_m = \frac{C_m}{C_{HPLC}} \cdot 100 \tag{12}$$

$$P_n = \frac{C_n}{C_{HPLC}} \cdot 100 \tag{13}$$

$$P_p = \frac{C_p}{C_{HPLC}} \cdot 100 \tag{14}$$

and

$$P_{n,p} = \frac{C_{n,p}}{C_{HPLC}} \cdot 100 \tag{15}$$

2.4.2. Model Reparameterization and Algorithm Improvement

In this study, we reparameterized the three-component model of PSCs based on in situ pigment measurements from the BS, the YS, and the ECS. According to section 2.1 and 2.2, 31 satellite match-ups of 178 surface samples were removed, leaving 147 samples for parameter establishment. The unknown model parameters $C_{n,p}^m$, C_p^m, $D_{n,p}$, and D_p were obtained by fitting the equations (14) and (15) using nonlinear least-square regressions (MATLAB R2014b, Curve Fitting Tool). The newly obtained parameters are shown in Table 3.

2.5. Error Tests

Different parameters of error tests were used to compare (1) the estimation of size-fractionated concentration and percentage from the different algorithms and in situ measurements; and (2) the size-fractionated concentration derived from satellite images and in situ measurements. These parameters include Pearson linear correlation coefficient (r), p-value (p), and the bias (δ) which was calculated by

$$\delta = \frac{1}{N}\sum_{i=1}^{N}(X_{i,A} - X_{i,B}) \tag{16}$$

where N is the number of samples and X is variable derived from A and B methods, respectively. In section 3.3, estimation from satellite data were regarded as A, and B was in situ HPLC measurements. Besides, mean absolute error (MAE) measures the average magnitude of errors in a set of comparison, while the root mean squared error (RMSE) represents the sample standard deviation of the differences between predicted values and observed values. Relative mean absolute error (MAE%) between in situ measurements and observations from satellite images is computed according to

$$\mathrm{MAE\%} = \left[\frac{1}{N}\sum_{i=1}^{N}\left|\frac{X_{i,A} - X_{i,B}}{X_{i,A}}\right|\right] \cdot 100 \tag{17}$$

where A is the in situ measurement and B is the estimation from satellite images.

3. Results

3.1. Total Chlorophyll-a Concentration and PSCs Derived From HPLC Pigments

Chlorophyll-a concentration (C_{HPLC}) ranged from 0.027 to 11.298 mg m^{-3} in the entire study area (Figure 2a). In the BS and the YS, the C_{HPLC} varied from 0.531 to 6.631 mg m^{-3}, and the average concentration was 1.849 mg m^{-3}. In the ECS, the C_{HPLC} had a wider range from 0.027 to 11.298 mg m^{-3}, with an average concentration of 0.454 mg m^{-3}. The C_{HPLC} was lower in the central BS, the northwest NYS, the central

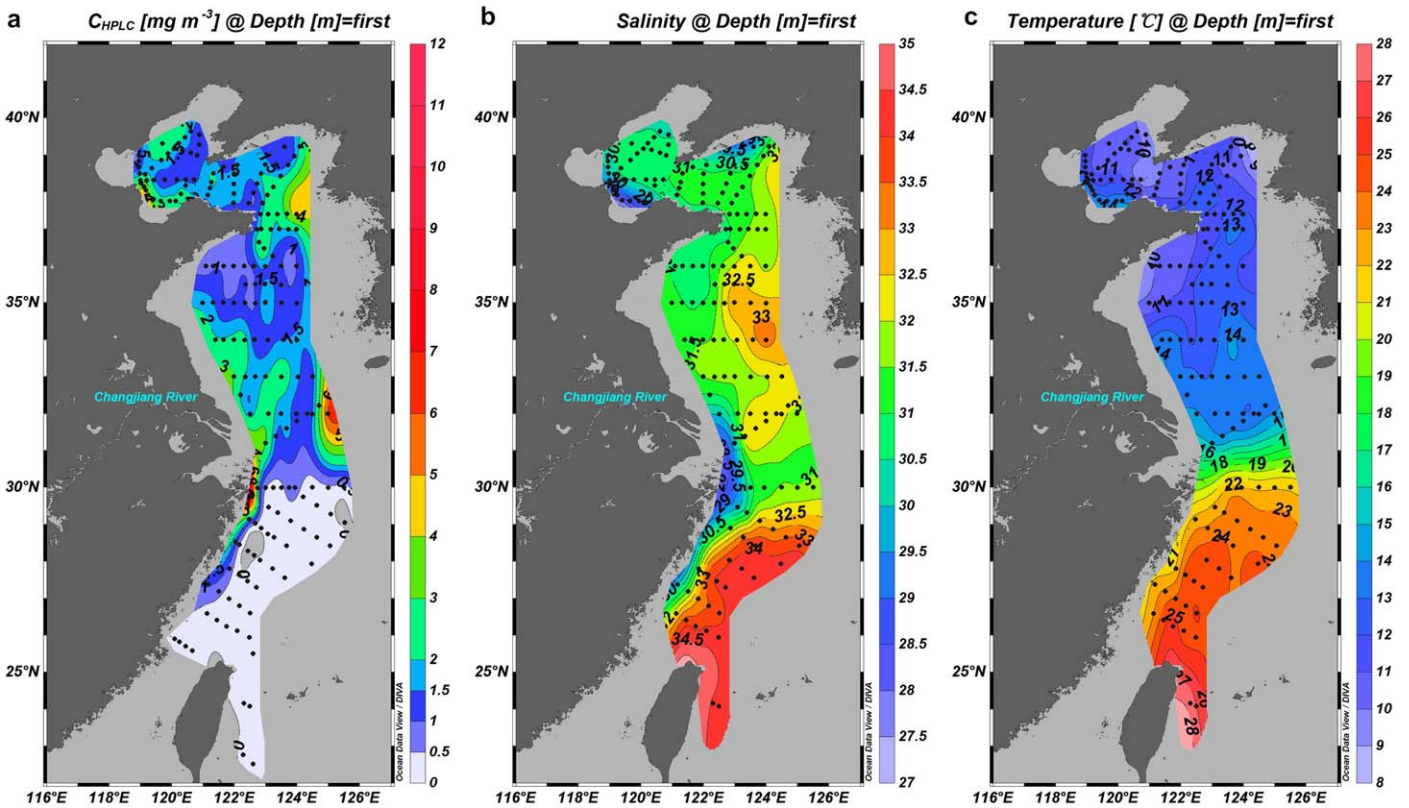

Figure 2. Distribution of surface (a) C_{HPLC}, (b) salinity, and (c) temperature in the Bohai Sea, the Yellow Sea, and the East China Sea during the 2014 cruise investigation.

SYS, and outer continental shelf area of the southeast ECS. By contrast, higher values were found in the coastal BS, the central NYS, coastal currents (i.e., Yellow Sea coastal current and Zhe-min coastal current) and the extension area of the Changjiang Diluted Water (CDW), which carries large quantities of freshwater from mainland and the salinity was less than 32.

Surface salinity and temperature ranged, respectively, from 27.95∼33.34 and 8.74∼14.79 (°C) in the BS and the YS (Figures 2b and 2c). Compared to temperature, salinity varied obviously from the nearshore area (i.e., northwest area of Shandong Peninsula and southeast area of Liaodong Peninsula) to the offshore area (i.e., central SYS). Higher salinities and temperatures were observed in the southeast of the ECS due to the influence of Kuroshio water and Taiwan warm current which transport high salinity and temperature surface waters to the eastern boundary of ECS, where the surface salinities and temperatures were 29.80∼34.46 and 21.58∼27.86 (°C), respectively. Salinities and temperatures were much lower in the nearshore area due to coastal currents and the CDW, compared to the offshore area.

The C_{HPLC}, salinity, and temperature had similar patterns of spatial distribution (Figure 2). In the nearshore area where salinity and temperature was lower, C_{HPLC} was higher, compared to the offshore area. With the increase of salinity and temperature, the C_{HPLC} tended to be lower. The C_{HPLC} had a negative relationship with salinity ($N = 35$, $r = -0.594$, $p < 0.001$) and temperature ($N = 35$, $r = -0.460$, $p < 0.01$) in the ECS.

Distribution of size-fractionated concentration of microplankton was similar to that of the C_{HPLC} (Figure 2a), having higher average value than nano and picoplankton, which were 1.116, 0.254, and 0.038 mg m^{-3}, respectively. In the nearshore area, both percentage and concentration of microplankton were higher than those of the other two groups (Figures 3a and 3d). Besides the central SYS, percentages of microplankton were higher than 70% in the BS and the YS. Nanoplankton was distributed extensively, especially in the ECS (Figures 3b and 3e), with the average percentage of 27.48% over the entire study area and 50.77% in the ECS. The percentage of picoplankton constituted the main background in the central SYS and offshore area

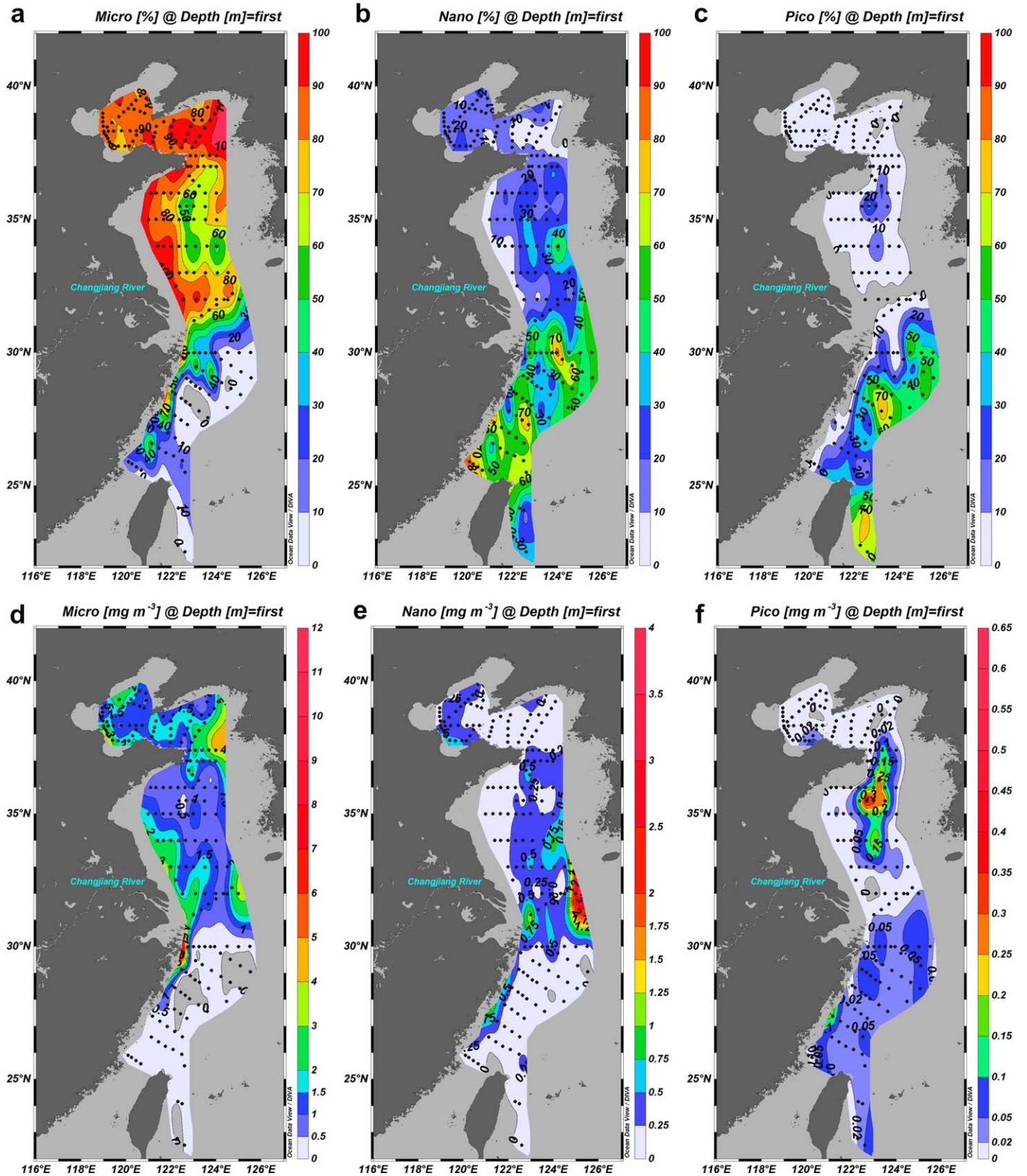

Figure 3. Spatial distribution of size-fractionated (a–c) percentages and (d–f) concentrations of micro, nano, and picoplankton in the Bohai Sea, the Yellow Sea, and the East China Sea during the 2014 cruise investigation.

in the ECS, where the C_{HPLC} was low (Figure 3c). For example, at station TW1–3-1 (24.08°N, 122.50°E) located east of Taiwan Island, the percentage of picoplankton was 78.54%. The concentrations of picoplankton were the lowest, which were no more than 0.1 mg m^{-3} in the most of the study area (Figure 3f).

When comparing size-fractionated percentages with the temperature and salinity, we found that in the BS and the YS, microplankton was negatively correlated with salinity (N = 123, $r = -0.361$, $p < 0.001$) and temperature (N = 123, $r = -0.379$, $p < 0.001$); nanoplankton was positively correlated with salinity (N = 123, $r = 0.275$, $p < 0.01$) and temperature (N = 123, $r = 0.362$, $p < 0.001$); and picoplankton had a positive correlation with temperature (N = 123, $r = 0.254$, $p < 0.01$). In the ECS, microplankton was negatively correlated with salinity (N = 35, $r = -0.414$, $p < 0.05$); picoplankton had positive correlation with salinity (N = 35, $r = 0.416$, $p < 0.05$) and temperature (N = 35, $r = 0.356$, $p < 0.05$).

3.2. PSCs Predicted by the Improved Algorithm

The improved algorithm (details in section 2.4.2) was applied to estimate concentrations and percentages of PSCs in the BS, the YS, and the ECS (Figure 4). Furthermore, estimates by other two algorithms from Brewin et al. (2010) and Hirata et al. (2011) are also shown in the plot, as a comparison. The size-fractionated percentages were smoothed with the 5-point running mean filer to improve the signal-to-noise ratio and make it easier to show changing regularities. The improved algorithm (red lines) fits the measurements well (Figure 4). The improved parameters were effective in predicting the trends in size-fractionated percentages of the PSCs in the BS, the YS, and the ECS, especially when chlorophyll-a concentration was high (Figures 4a–4d). As for concentrations, the improved algorithm had good agreements in estimating microplankton and nanoplankton. Because of the extremely low values of picoplankton in the BS and the YS (Figures 3f and 4h), the improved algorithm had lower precision in estimating picoplankton concentration when chlorophyll-a concentration was high, and its trend with the change of total concentration requires further study.

For the purpose of discussing the applicability of two existed methods (details in section 4.1), PSCs derived from three component model (Brewin et al., 2010) and from empirical equations (Hirata et al., 2011) were shown as well. Instead of estimating size-fractionated concentration (Brewin et al., 2010), Hirata et al. (2011) expressed the percentages of PSCs (P_m, P_n, and P_p) instead of concentration. The equations are

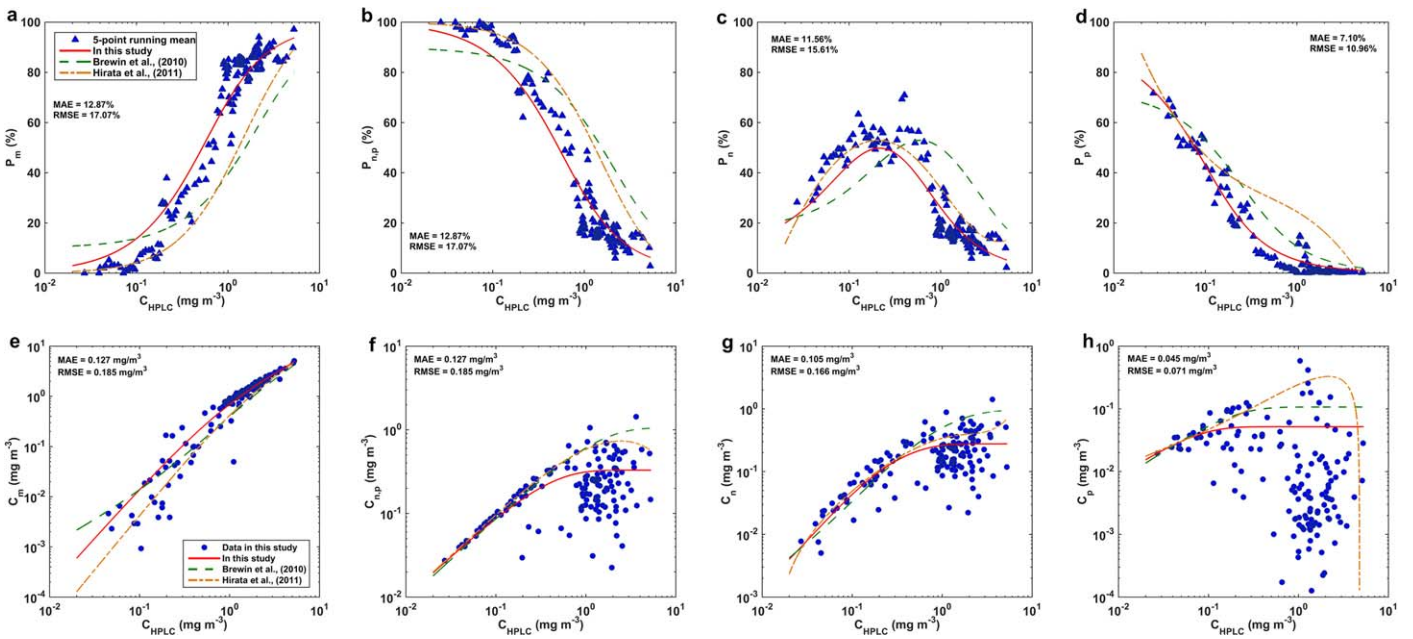

Figure 4. Relationships between size-fractionated (a–d) percentages and (e–h) concentrations, all as a function of C_{HPLC}. Measurements included in situ data (blue dots) and 5-point running mean data (blue triangles), $N = 149$. Estimations were predicted by the improved algorithm in this study (red lines), by Brewin et al. (2010) (green dotted lines) and by Hirata et al. (2011) (yellow dash dot lines). MAE and RMSE were calculated between in situ measurements and estimations from the improved algorithm.

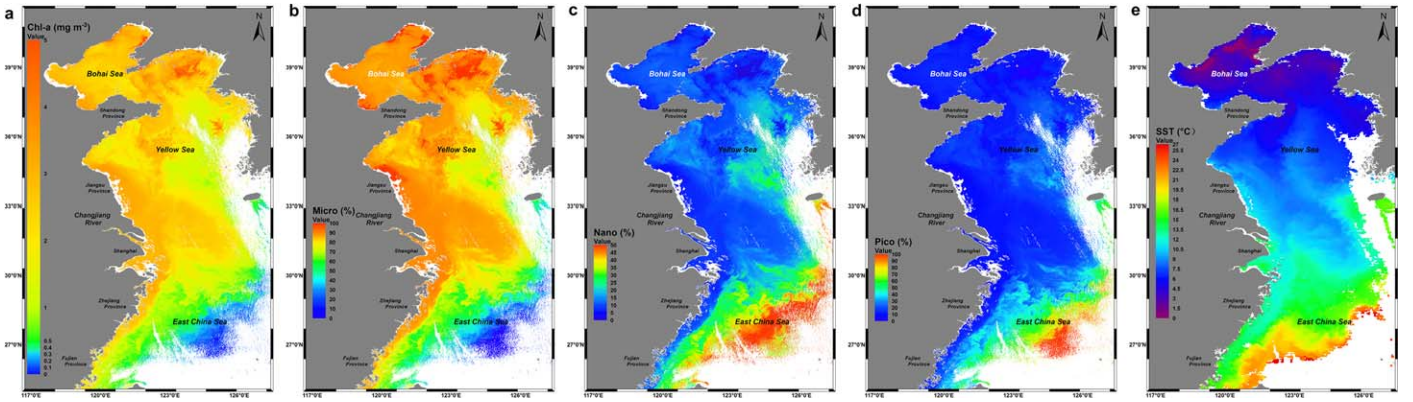

Figure 5. GOCI-derived chlorophyll-a concentration (a, Chl-a, in unit of mg m^{-3}) and percentage (%) of each PSCs (b–d) in the Bohai Sea, the Yellow Sea, and the East China Sea, which were estimated by the improved algorithm. The GOCI image was taken at 10:28 on 7 April 2013 (Beijing time). Daily sea surface temperature image of SNPP VIIRS (e, in unit of °C) on the same day.

$$P_m = (0.9117 + \exp(-2.7330 \cdot \log_{10}(C_{HPLC}) + 0.4003)^{-1} \cdot 100 \quad (18)$$

$$P_n = 100 - P_m - P_p \quad (19)$$

and

$$P_p = \{-[0.1529 + \exp(1.0306 \cdot \log_{10}(C_{HPLC}) - 1.5576)]^{-1} - 1.8597 \cdot \log_{10}(C_{HPLC}) + 2.9954\} \cdot 100 \quad (20)$$

the concentration of each PSCs can be calculated by multiplying its percentage by the total, which are C_m, C_n and C_p.

3.3. GOCI-Derived PSCs and Validation

All the GOCI images with less cloud coverage from April to June from 2011 to 2017 were processed, of which images on 7 April 2013 had the best image quality and the largest available areas. Figure 5 showed the spatial distributions of the chlorophyll-a concentration and the estimation of size-fractionated percentages by the improved algorithm, which were derived from the GOCI image at 10:28 (center time of the scene, Beijing time) on 7 April, 2013. Daily SNPP VIIRS sea surface temperature on the same day was shown as well.

Figure 5a illustrated that higher values of chlorophyll-a concentration distributed in the northern BS, northern NYS, central SYS, and along the nearshore area of the YS and the ECS. While in the offshore area, such as the eastern SYS and the southeastern ECS, concentrations were much lower. The distribution pattern of microplankton percentage was similar to the total concentration. Except for the offshore area of the ECS, microplankton was dominant in the study area where chlorophyll-a concentrations were higher than 1 mg m^{-3} (Figure 5b). Nanoplankton had lower percentage in the BS and nearshore area of the YS and the ECS, while in the offshore area of the SYS and the ECS, its percentage ranges from 20% to 50% (Figure 5c). By contrast, picoplankton only had higher distribution in the offshore area and percentage in these areas tended to be greater than 40% (Figure 5d). Figure 5e showed that temperature rose from north to south and from west to east in the study area, due to the influence of Taiwan warm current, the Kuroshio and its brunches. Temperature in the offshore area of the SYS and the ECS was higher, leading to lower percentage of microplankton and higher percentages of nano and picoplankton. In comparison, distribution of total chlorophyll-a concentration and microplankton percentage had clear negative correlation with temperature, while nanoplankton and picoplankton percentages were positively correlated to temperature. This estimated distribution of PSCs' derived from the GOCI image with the improved algorithm had a good consistency with the in situ results presented in section 3.1, especially for the BS and the YS, where both the image time and the investigation time were in April. However, the shaded area caused by the shape of clouds, leading to challenges in representing full knowledge of PSCs in the study area, especially for the edges. Additionally, there is a temporal limitation in observing continuous changes with one image.

Table 4
Comparison of Chlorophyll-a Concentration Between In Situ Measurements and Observations Derived From Satellite Data Using Different Chlorophyll-a Concentration Algorithms (N = 31)

	δ (mg m^{-3})	MAE (mg m^{-3})	RMSE (mg m^{-3})	MAE% (%)
OC2	0.368	0.720	0.928	69.00
YOC (preprocessing)	0.408	0.698	0.974	55.75
YOC (postprocessing)	−0.050	0.626	0.824	43.83

The improved algorithm was then applied to GOCI images to validate the estimation accuracy of PSCs through independent match-ups between satellite data and in situ measurements. During the investigation time, 31 in situ data were matched to the GOCI satellite images. In the GDPS (version 1.4.1), there are three algorithms for chlorophyll-a concentration retrieval, of which OC2 (ocean chlorophyll 2 algorithm) and YOC algorithms were selected for comparison. Based on the data set from oceanic waters, OC2 proposed by O'Reilly et al. (1998) was the default for chlorophyll analysis in the GDPS, whereas the YOC data set from Siswanto et al. (2011) covered the YS and the ECS. Chlorophyll-a concentrations derived directly from GDPS using YOC algorithm were named YOC (preprocessing). Considering the mosaic edge effects caused by Band 1 at 412 nm in L1B products, a neighboring pixel interpolation method was used (details in section 2.2) in processing chlorophyll-a concentration, thus using YOC (postprocessing) to distinguish from YOC (preprocessing). Statistically, the YOC algorithm was better than the OC2 algorithm in the study area, as it had lower bias, MAE, RMSE, and MAE% (Table 4).

Based on the images with neighboring pixel interpolation processing, independent satellite and in situ match-up data (N = 31) were compared, including chlorophyll-a concentration, size-fractionated concentration, and size fractionated percentages. When calculating errors, extremely low in situ size-fractionated concentrations which less than 0.01 mg m^{-3} were eliminated, leaving 29, 31, and 18 match-ups for micro, nano, and picoplankton. Figure 6a showed that satellite-derived total and microplankton chlorophyll-a concentration had good agreements with in situ measurements, with MAE% of 43.83% and 49.09%, respectively. Biases indicated that the improved algorithm overestimated microplankton concentration and underestimated nanoplankton concentration slightly. As for picoplankton concentration, poor MAE%

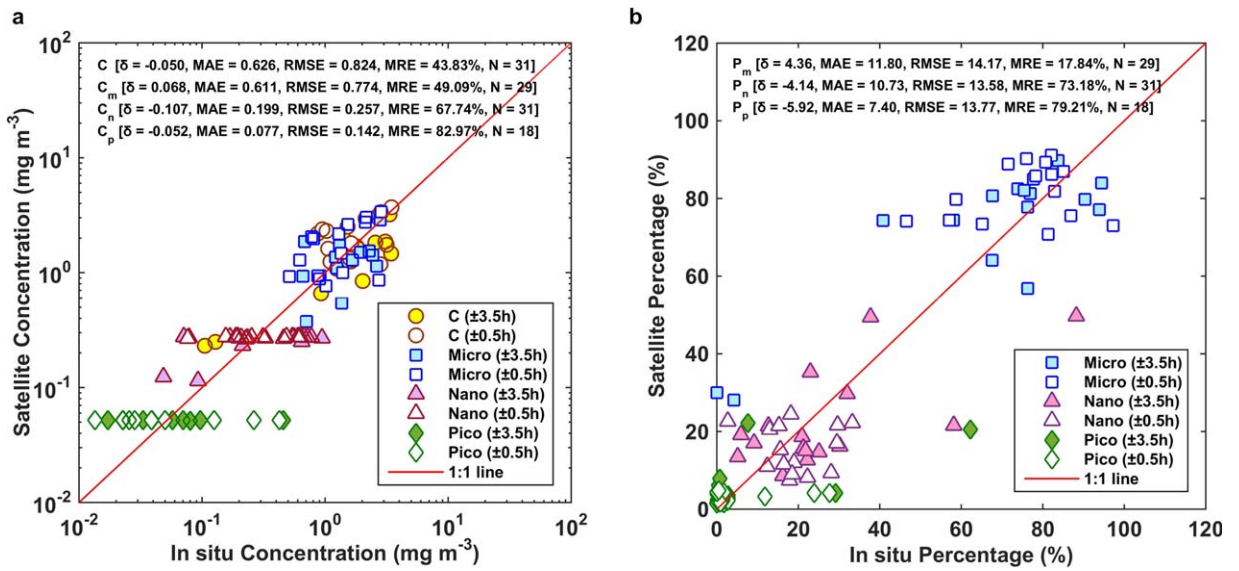

Figure 6. Validation of GOCI estimations using the improved algorithm through match-ups, including (a) total chlorophyll-a concentration (yellow circle) and size-fractionated chlorophyll-a concentration of micro (blue square), nano (purple triangle) and picoplankton (green diamond), and (b) size fractionated percentages of micro, nano, and picoplankton. Match-ups within ±3.5 h are shown in filled symbols, while match-ups within ±0.5 h are shown in empty symbols. Solid lines represent the 1:1 lines. The units of δ, MAE, RMSE are mg m^3 in Figure 6a, and % in Figure 6b.

(82.97%) was obtained compared to the other groups, which was caused by the limited coverage of match-ups. Match-ups mostly distributed in the BS and the YS (Figure 1), where microplankton was dominant during the investigation and in situ picoplankton concentrations were low (Figures 3c and 3f). By contrast, picoplankton was abundant in the offshore ECS, however, cloudy weather was common during the ECS cruise and only two match-ups were found in the ECS. Figure 6b showed that the improved algorithm had a better accuracy in estimating the microplankton percentage (MAE% = 17.84%), while it underestimated percentages of nano and picoplankton, compared to the in situ measurements. Moreover, match-ups within ±0.5 h (empty symbols) were shown in the Figure 6 as well, and with this strict time window, the improved algorithm had a better accuracy in estimating PSCs, with the RMSE for size-fractionated chlorophyll-a concentrations and percentages are 0.848, 0.183, 0.139, and 14.48, 10.60, 10.14, respectively.

3.4. Diurnal Surface Variation of GOCI-Derived Chlorophyll-a and PSCs

Diurnal variation of chlorophyll-a and PSCs were derived from GOCI images on 7 April, 2013 from 8:28 to 15:28 (center time of the scene, Beijing time). Based on the available coverage of eight images, a transect and four regions of interest were analyzed, which are ROI-1 (center coordinate, 34.33°N, 123.15°E), ROI-2 (29.96°N, 122.56°E), ROI-3 (29.80°N, 122.94°E), and ROI-4 (29.62°N, 123.39°E), 11 pixels by 11 pixels (Figures 7a and 7b). ROI-1 is located far away from the coast, less affected by coast currents and contains clearer water. The transect in the southeastern area of Zhoushan Island is approximately parallel with the direction of tidal currents and vertical to isobaths. Due to the impacts of different water masses and current systems,

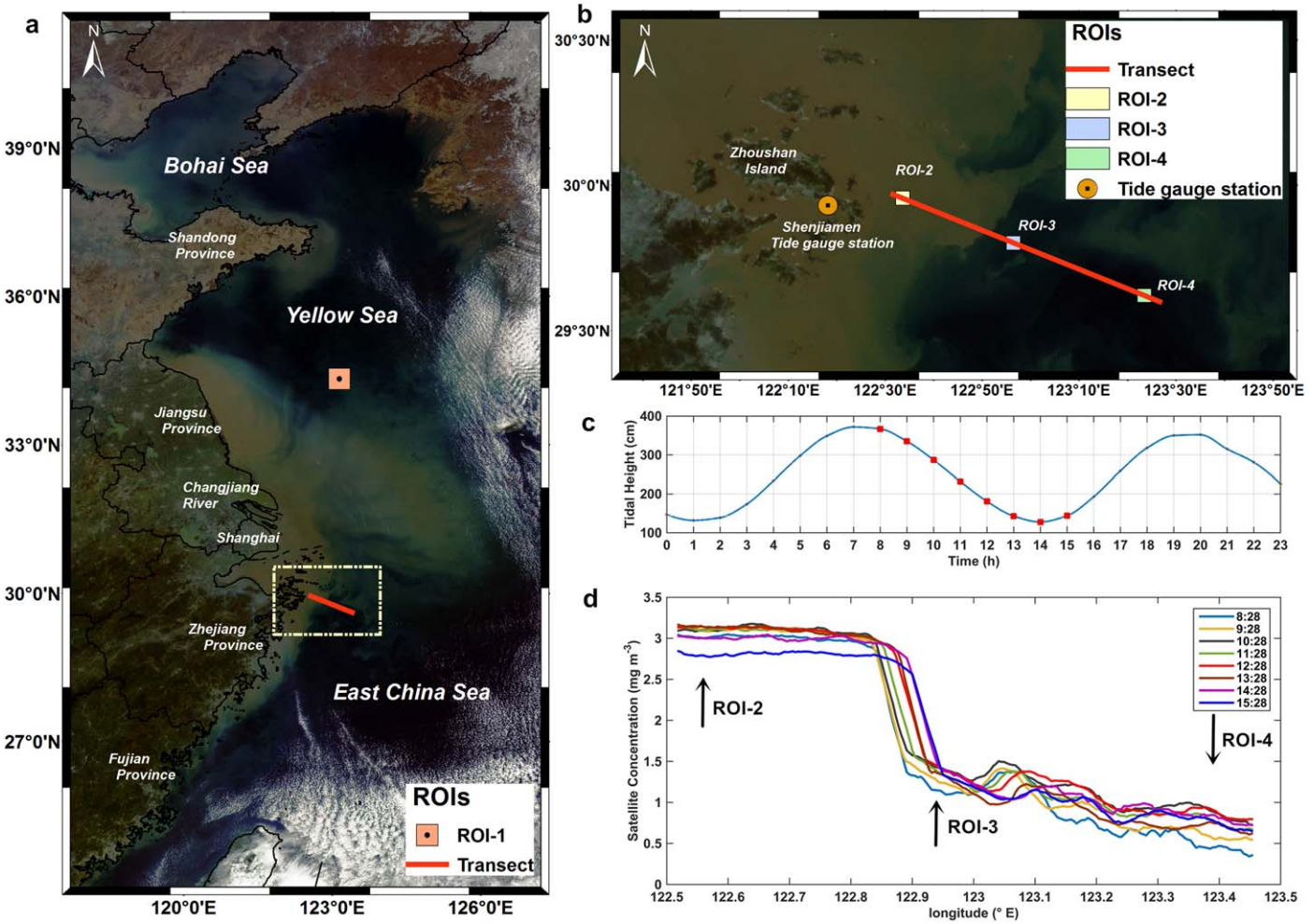

Figure 7. A transect and four regions of interest (ROIs) utilized in diurnal variation (a, b). The base map is a three-band composite true color image acquired at 10:28 (local time, red: Band 6, green: Band 4, blue: Band 2). (c) Tide height from Shenjiamen tide gauge station on 7 April 2013, the red squares represent hourly imaging time of GOCI images. (d) Diurnal variation of GOCI-derived chlorophyll-a concentration of the transect.

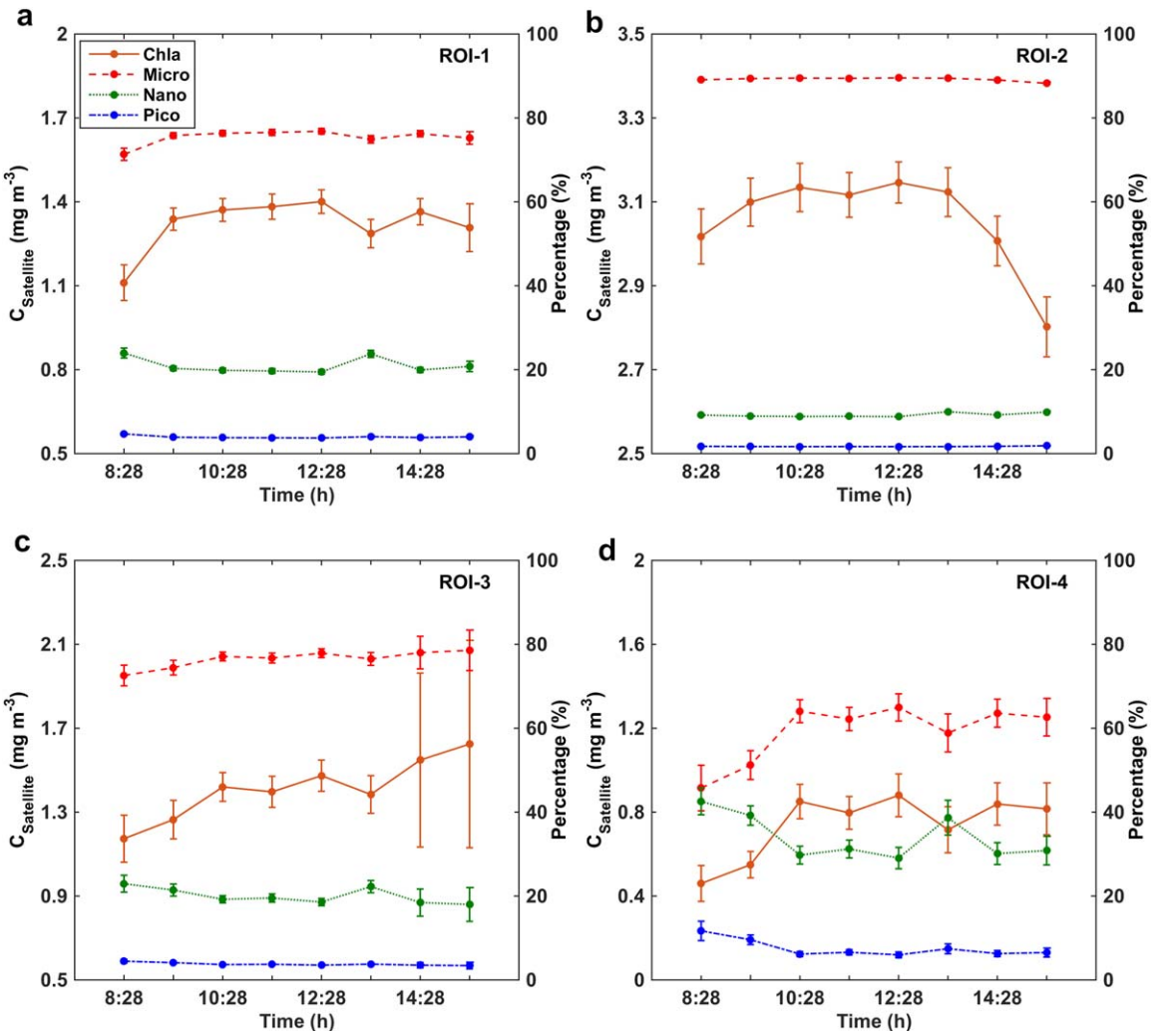

Figure 8. Diurnal surface variations of GOCI-derived chlorophyll-a concentration (mg m^{-3}) and percentage of PSCs (%) are included in (a) ROI-1, (b) ROI-2, (c) ROI-3, and (d) ROI-4. The axis on the left gives the concentration (mg m^{-3}) and the axis on the right gives the percentage (%) and deviation bar were included for chlorophyll-a concentration and percentages of PSCs.

chlorophyll-a concentration of the transect decreased obviously from nearshore area to offshore area (Figure 7d). Besides, characteristics of diurnal variation changed with the distance from the shore. Thus, ROI-2, ROI-3, and ROI-4 were extracted, located at nearshore area, the transition region with a steep drop in chlorophyll-a concentration and offshore area, respectively.

GOCI-derived chlorophyll-a values showed a regular pattern of variation during the daytime (Figures 8a, 8b, and 8d). In the morning, the concentration value was the lowest, after that it reached its highest value between 10:00 and 12:00. Then in the afternoon, the concentration tended to decline. However, due to the impact of tides, variation of chlorophyll-a concentration in the afternoon was different in the transition area (i.e., ROI-3). Diurnal variations in four ROIs were as follows.

1. In the ROI-1, chlorophyll-a value varied from 1.11 to 1.40 mg m^{-3} throughout the day and peaked at 12:28 (Figure 8a). Microplankton was the major component throughout the day, while nanoplankton had higher percentages in the morning and afternoon. Picoplankton was no more than 5% throughout the day.
2. Since the ROI-2 received more terrestrial inputs, chlorophyll-a concentration was the highest among four ROIs, ranging from 2.80 to 3.15 mg m^{-3} during the daytime (Figure 8b). Microplankton was dominant, while percentages of nanoplankton and picoplankton were less than 10% during the daytime.

Table 5
Comparison of Size-Fractionated Percentages and Concentrations Between In Situ Measurements and Estimations From Three Methods in Different Study Areas

			Percentage (%)			Concentration (mg m^{-3})		
Method	Study area	Error tests	Micro	Nano	Pico	Micro	Nano	Pico
Brewin et al. (2010)	Entire area	MAE	25.36	23.53	10.33	0.337	0.288	0.079
	N = 147	RMSE	29.87	26.03	13.33	0.434	0.367	0.096
Hirata et al. (2011)	Entire area	MAE	21.24	13.41	17.44	0.271	0.135	0.185
	N = 147	RMSE	27.07	16.48	19.13	0.352	0.187	0.221
In this study	Entire area	MAE	12.87	11.56	7.10	0.127	0.105	0.045
	N = 147	RMSE	17.06	15.61	10.96	0.185	0.166	0.071
In this study	BS and YS	MAE	10.63	7.83	4.22	0.162	0.129	0.058
	N = 93	RMSE	13.22	9.94	7.28	0.208	0.183	0.085
In this study	ECS-1	MAE	23.34	21.74	12.51	0.136	0.129	0.037
	N = 19	RMSE	29.43	26.86	17.04	0.225	0.211	0.047
In this study	ECS-2	MAE	13.13	15.94	11.82	0.027	0.029	0.018
	N = 35	RMSE	16.99	19.23	14.35	0.044	0.046	0.023

Presumably nutrient concentrations would provide enhanced growth conditions for microplankton. Size-fractionated percentages were stable within the day and insensitive to environmental changes.

3. As for the ROI-3, the biggest difference was that chlorophyll-a concentration increased at 14:28 and 15:28 (Figure 8c). As shown in the Figure 7c, all the eight images were acquired during the ebb tide phase when water flowed from nearshore area to offshore area. Under the influence of the tidal currents, high chlorophyll-a concentration nearshore move southeastward to the offshore area, as well as high percentages of microplankton. The increasing temperature and decreasing turbidity led to higher percentages of nanoplankton and picoplankton in this region, compared to the ROI-2.
4. The variation trend of chlorophyll-a concentration in the ROI-4 was similar to that in the ROI-1. However, chlorophyll-a concentrations were much lower, ranging from 0.46 to 0.88 mg m^{-3} (Figure 8d). Both microplankton and nanoplankton were dominant groups and picoplankton percentage was higher than 10% at 8:28. Percentages of nano and picoplankton decreased with the light intensity increased. The intrusion of Taiwan warm current with high temperature and salty water masses made it beneficial for the growth of small size phytoplankton.

In summary, characteristics of spatial distributions of PSCs were affected by environmental factors and diurnal variations were observed as well, which will be discussed later.

4. Discussion

4.1. Applicability of Methods for Deriving PSCs

By comparison, the improved algorithm had an advantage in estimating both percentages and concentrations of PSCs (Figure 4 and Table 5). When chlorophyll-a concentration was low, percentage and concentration of microplankton derived from Hirata et al. (2011) were more suitable to in situ measurements since there was an acceleration in the regression slopes (Figure 4a). However, when chlorophyll-a concentration was high, it underestimated. The three-component model (Brewin et al., 2010) had lower accuracy in estimating microplankton, with a little bit higher MAE and RMSE (Table 5). As for estimating nanoplankton and picoplankton, three methods had differences (Figures 4c, 4d, 4g, and 4h). Both algorithms of Brewin et al. (2010) and Hirata et al. (2011) seemed to overestimate nanoplankton and picoplankton when chlorophyll-a concentration was high, which made it less applicable in the study area. Since the three-component model is based on an underlying conceptual model (Sathyendranath et al., 2001), it was parameterized to fit the study area. As a result, the improved algorithm has a higher estimation accuracy.

Moreover, due to the effects of CDW and Zhe-min coastal current, the ECS was divided into two parts, one is the area where salinity was lower than 32 (ECS-1), the other is the outer continental area where salinity was higher than 32 (ECS-2). Table 5 showed that the improved algorithm had a better accuracy in estimating PSCs in the BS and the YS, since more measurements were utilized in parameterization and

environmental factors were homogeneous relatively (Figures 2b and 2c). In the ECS, abundant fresh water and nutrients carried by the coastal current supported the growth of large size phytoplankton (Deng et al., 2008; Huang et al, 2006; Sun et al., 2012), which affected the distribution of PSCs, making the model less robust in the nearshore area (ECS-1). Without the influence of the coastal current, the improved algorithm provided a better estimation in the ECS-2.

4.2. Spatial Distribution of PSCs

GOCI-derived PSCs' distribution showed that microplankton and nanoplankton were generally the major contributors to coastal and transitional regions, and picoplankton was found to be abundant in the oligotrophic regions (Figure 5), which was consistent with in situ investigations in our study (Figure 2), previous studies in the BS, the YS, and ECS (e.g., Fu et al., 2009; Huang et al, 2006; Sun et al., 2002, 2012), and from other study areas (e.g., Arin et al., 2002; Chisholm et al., 1988; Madariaga & Orive, 1989; Marañón et al., 2001). Similar distribution of GOCI-derived PSCs was observed from our study (Figure 5) and the study of Sun et al. (2017). However, slight differences existed in the nearshore BS and SYS where microplankton instead of nano and picoplankton was dominant in our study, which might result from regional data sets for modeling and time scales utilized in the two studies.

Spatial distribution is closely related to the competitive abilities of different PSCs in response to environmental conditions. Figures 2b and 2c showed that salinity and temperature were higher in the central YS and the offshore ECS, due to the influence of Yellow Sea warm current, Taiwan warm current, and Kuroshio (Li et al., 2016; Quan et al., 2013; Yu et al., 2005). Results in section 3.1 revealed that temperature and salinity were correlated to the phytoplankton size structure, which might serve to explain why nano and picoplankton had higher concentrations and percentages offshore. Similar correlations were observed in a previous study in the same season and area (Sun et al., 2012). However, obvious relationships between PSCs and temperature or salinity in the YS and the ECS were not found from Deng et al. (2008), indicating that environmental factors that determined the PSCs were more than temperature and salinity. Some previous studies have suggested that nutrients have positive correlations with larger phytoplankton and negative correlations with smaller phytoplankton in the YS and the ECS (Deng et al., 2008; Sun et al., 2012). Indeed, higher dissolved inorganic nitrogen, phosphate, and silicate along coastlines and in the Changjiang Estuary and its adjacent areas were observed (Gong et al., 2003; Guo et al., 2014; Liu et al., 2015; Wang et al., 2003; Zhang et al., 2007), supporting our results that micro and nanoplankton were distributed with higher percentages in nearshore areas (Figure 3). With the enhanced solar radiation in April, sea surface temperature increased and the stratification occurred in the central YS (Li et al., 2016; Yu et al., 2005), preventing the supplementary of nutrients in the surface. Availability of nutrients became the major limiting factor for the growth of large-sized phytoplankton in more oligotrophic environments (Marañón, 2015). Due to the surface-area-to-volume ratio, small cells are considered to be more competitive under limiting nutrient conditions (Agawin et al., 2000; Marañón et al., 2013), which could help to explain why percentage and concentration of picoplankton were higher in the central YS (Figures 3c and 3f).

4.3. Diurnal Variation of PSCs

Unlike polar-orbiting ocean color satellites (e.g., SeaWiFs and MODIS), GOCI has higher temporal resolution which can capture diurnal changes. Plenty of researches showed applications in suspended particulate materials (Ge et al., 2015; He et al., 2013; Pan et al., 2018) and phytoplankton (Choi et al., 2014; Lee et al., 2012; Lou & Hu, 2014). The atmospheric correction utilized in this study (i.e., KOSC standard in GDPS system) is the same as that in the researches of diurnal variation of turbidity fronts (Hu et al., 2016a), tidal currents (Hu et al., 2016b), and salinity (Liu et al., 2017).

Hourly variations of chlorophyll-a concentration observed from space were obvious throughout the day in all the ROIs (Figure 8). Maximum chlorophyll-a concentration usually occur around noon, which was similar with the temporal pattern from Lorenzen (1963) and Maulood et al. (1978). Similar trends of variation between photosynthetically available radiation (PAR) and chlorophyll-a concentration among the four ROIs indicated that the diurnal variation of chlorophyll-a concentration might due to the ability of photosynthesis to light by phytoplankton (Figures 8 and 9a). Synchronous GOCI-derived PAR was calculated by

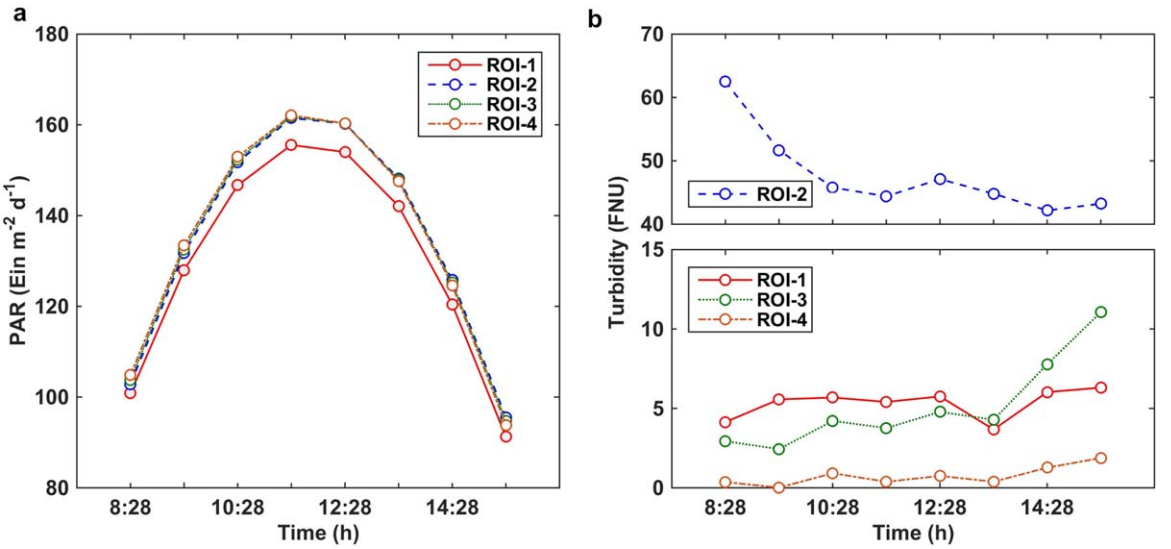

Figure 9. GOCI-derived diurnal variation of (a) photosynthetically available radiation (PAR) and (b) turbidity in the four ROIs.

$$\mathrm{PAR}=\sum_{i=1}^{5}\frac{\lambda_{i+1}-\lambda_i}{hc}\,\frac{\lambda_i E_{\mathrm{d}}(\lambda_i)+\lambda_{i+1}E_{\mathrm{d}}(\lambda_{i+1})}{2} \tag{21}$$

where $\lambda_i = 412$, 443, 490, 555, 660, and 680 nm, $h = 6.626*10^{-34}$ j s, $c = 2.996*10^{8}$ m s^{-1}, $E_{\mathrm{d}} = L_{\mathrm{w}}/R_{\mathrm{rs}}$ and the unit of PAR was convert to Ein m^{-2} d^{-1}. The equation (21) is originated from Cao and Yang (2002).

As for PSCs, variations were much stronger in the offshore area. It is obvious that the percentages of microplankton increased with the increasing radiation, while the picoplankton was opposite (Figures 8a and 8d). Previous study found that micro and nanoplankton required more illuminance intensity than picoplankton for reaching the best growth condition (Sun et al., 2008). Dinoflagellates, such as *Ceratium tripos* and *Ceratium furca* were phototactic and had characteristics of diurnal vertical migration (i.e., upward migration to the surface in the morning and downward migration in the evening), leading higher abundance in the upper layers during the daytime (Blasco, 1978; Jephson & Carlsson, 2009). By contrast, small cells cope better with reduced light conditions, since they are less affected by the package effect (Finkel et al., 2004). Surface chlorophyll and abundance of *Synechococcus* were observed higher in the morning and after evening, while at noon the lower populations could be suffered from photoinhibition because of the high radiation (Mitbavkar & Saino, 2015; Vaulot & Marie, 1999). Since the phytoplankton mentioned above are common species in the ECS (Chen et al., 2006), their responses to the light can well explain the features of surface distribution in this study.

Furthermore, water turbidity is one of important factors for phytoplankton in turbid coastal oceans. Figure 9b showed GOCI-derived hourly turbidity of the four ROIs, which was computed following equations from Dogliotti et al. (2015). Compared to the ROI-1 which was located far from the coast, diurnal variations were more obvious in the ROI-2, ROI-3, and ROI-4. Turbidity was the highest in the ROI-2, where suspended particulate matters were mainly dominated by nonalgal particles. Under influences of tidal currents, coastal currents, and waves, the mechanism of the turbidity variation was complicated, and the relationship between turbidity and chlorophyll-a concentration was not significant. Diurnal variations of PSCs in the ROI-2 were stable and less affected by environmental factors (Figure 8b). The ROI-3 was located in turbid-clear transition zone. Diurnal variation of turbidity might be influenced by the tidal current. It was found in Figure 9b that an obvious increment of turbidity was found in the afternoon, which was corresponding to the ebb tidal phase of 7 April 2013 (Figure 7c). Horizontal transportation of the water mass was the cause of the variation in chlorophyll-a concentration and percentages of PSCs in the afternoon (Figure 8c). Diurnal variation of bloom surface distribution impacted by tidal situation in nearshore waters of ECS was also reported by Lou and Hu (2014). The ROI-4 was situated in the clearer water mostly dominated by high salinity and oligotrophic water mass of Taiwan warm current so that it had the lowest turbidity, where algal particles were the major component of suspended particulate matters. Thus, the fluctuation of turbidity suggested the

variation of chlorophyll-a concentration (Figures 8d and 9b). Compared to other ROIs, percentages of PSCs had significant variations in the ROI-4 within a day due to the combined effects of both light intensity and turbidity. In addition to environmental factors mentioned before, intrinsic population processes caused by resuspension of benthic phytoplankton and grazing might also have influences on diurnal variation of PSCs. Consistent and more comprehensive monitoring in the whole water column is required in the future.

4.4. Potential and Limitation of Remote Sensing Estimation

In general, PSCs can be detected by remote sensing through three popular approaches—abundance-based, spectral-based, and ecological-based (Brewin et al., 2011b; IOCCG, 2014; Nair et al., 2008). The three-component model (Brewin et al., 2010) which is regarded as an abundance-based method can be used to estimate PSCs when chlorophyll-a concentration derived from space has been proved to be accurate. The accuracy of classification is completely relied on parameters in the models, thus model parameters are required to improve for different biogeochemical provinces (Devred et al., 2006). In this study, parameters of the model were tuned and validated according to our investigation. However, the abundance-based approach has its limitations that it might not work well in distinguishing algal blooms of different PSCs with the same chlorophyll concentration, since it assumes that larger cells dominate in higher concentrations and smaller cells in low concentrations. Many studies found that microplankton such as dinoflagellates were the most common dominances along coastal waters in the study area (e.g., Dai et al., 2013; Lou & Hu, 2014; Xia et al., 2007; Zhou et al., 2003) which confirmed the assumptions of the abundance-based model. Although there are few reports, there is the possibility that small size or mixed sizes phytoplankton blooms could exist. Therefore, bloom stations were removed in the reparameterization in the study. When analyzing PSCs in blooming conditions utilizing the abundance-based approach, additional environmental knowledge are required to improve the model reliability (Brewin et al., 2010).

In order to be more dependable, recent trend of detecting PSCs concerned more about the comparison and combination of different approaches. Spectral-based approach is a more direct way depending on features that spectrum shape of chlorophyll-specific absorption coefficient or particle backscattering coefficient varies with size structure (Brewin et al., 2011a; Ciotti & Bricaud, 2006; Ciotti et al., 2002; Kostadinov et al., 2009; Loisel et al., 2006; Uitz et al., 2008). Brewin et al. (2011b) has proved that both abundance-based and spectral-based approaches can have similar accuracy, however, comparison results remain to be tested in the BS, the YS, and the ECS. As discussed in the section 4.2, environmental factors are crucial to the distribution pattern of PSCs, and several studies have pointed that some of them, such as light availability and temperature are tightly related to parameters of abundance-based model (Brewin et al., 2015, 2017). The combination of empirical methods and the exploitation of additional environmental data will help to optimize models and obtain retrivals more accurately (Bracher et al., 2017).

5. Conclusions

Large numbers of in situ samples were collected in the entire continental shelf sea of China. Through the HPLC method, seven diagnostic pigments were obtained and assigned to corresponding size classes. In situ PSCs' distributions showed that microplankton was dominant in the BS, the YS, and nearshore ECS, while nanoplankton was the major contribution to the chlorophyll-a concentration in the ECS, and picoplankton had higher proportions in the offshore ECS. Temperature and salinity in the study area affected by continental shelf currents circulation had influences on the spatial distribution of PSCs. Microplankton was negatively correlated with the temperature and salinity, while nano and picoplankton had positive correlations.

We proposed an improvement on the parameterization of the three-component model (Brewin et al., 2010). Using strict match-ups, validation revealed that the improved algorithm had a higher accuracy in estimating PSCs in the BS, the YS, and the ECS, with RMSE of concentrations and percentages been 0.774, 0.257, 0.142, and 14.17, 13.58, 13.77 for micro, nano, and picoplankton, respectively.

GOCI-derived PSCs' spatial distribution was in good agreement with in situ measurements and previous studies, resulting from responses of PSCs to different environmental conditions. Characteristics of diurnal variations of PSCs' distributions in different water types were captured by this high temporal resolution satellite as well. Diurnal variation of PSCs in the offshore area was obvious and mainly affected by the light intensity, leading to maximum microplankton percentage around noon and higher percentages of nano

and picoplankton in the morning and afternoon. However, in the nearshore area, diurnal variation of PSCs was relatively slight and water masses such as coastal currents and tides were major influencing factors. The study provides a beneficial approach of a consistently spatial-temporal observation of PSCs for better understanding marine ecological and biogeochemical systems in the entire continental shelf sea of China.

Acknowledgments

This work is supported by National Key R&D Program of China (2016YFE0103200), NSFC projects (41771378), and SKLEC-2016RCDW01. We would like to thank the KORDI/KOSC for providing GOCI data (http://kosc.kiost.ac/eng/) and NASA Ocean Color for providing SNPP VIIRS data (https://oceancolor.gsfc.nasa.gov/). In situ water sample data in the Bohai Sea, Yellow Sea, and East China Sea in 2014 were obtained from the "Dongfanghong 2" and "Kexue 1" cruise campaigns and all the scientists and crew who participated in the field surveys are sincerely appreciated. Data sets utilized in this study has been publicly available at https://figshare.com/s/65f0cbe1ed8932dafeb0. We are grateful to the team of Bangqin Huang from Xiamen University for helping with the laboratory analysis of HPLC pigment concentrations in the East China Sea and Jingjing Zhang from Yantai Institute of Coastal Zone Research for collection and laboratory analysis of HPLC pigment concentrations in the Bohai Sea and Yellow Sea in this work. The authors also greatly appreciate Michael A. St. John for instructive comments on the earlier versions of the manuscript and anonymous reviewers for their constructive comments and suggestions.

References

Agawin, N. S. R., Duarte, C. M., & Agustí, S. (2000). Nutrient and temperature control of the contribution of picoplankton to phytoplankton biomass and production. *Limnology and Oceanography*, *45*(3), 591–600. https://doi.org/10.4319/lo.2000.45.3.0591

Arin, L., Morán, X. A. G., & Estrada, M. (2002). Phytoplankton size distribution and growth rates in the Alboran Sea (SW Mediterranean): Short term variability related to mesoscale hydrodynamics. *Journal of Plankton Research*, *24*(10), 1019–1033. https://doi.org/10.1093/plankt/24.10.1019

Aumont, O., Maier-Reimer, E., Blain, S., & Monfray, P. (2003). An ecosystem model of the global ocean including Fe, Si, P colimitations. *Global Biogeochemical Cycles*, *17*(2), 1060. https://doi.org/10.1029/2001GB001745

Behrenfeld, M. J., & Boss, E. S. (2014). Resurrecting the ecological underpinnings of ocean plankton blooms. *Annual Review of Marine Science*, *6*(6), 167–194. https://doi.org/10.1146/annurev-marine-052913-021325

Blasco, D. (1978). Observations on the diel migration of marine dinoflagellates off the Baja California coast. *Marine Biology*, *46*(1), 41–47. https://doi.org/10.1007/BF00393819

Bracher, A., Bouman, H. A., Brewin, R. J. W., Bricaud, A., Brotas, V., Ciotti, A. M., et al. (2017). Obtaining phytoplankton diversity from ocean color: A scientific roadmap for future development. *Frontiers in Marine Science*, *4*, 55. https://doi.org/10.3389/fmars.2017.00055

Brewin, R. J. W., Ciavatta, S., Sathyendranath, S., Jackson, T., Tilstone, G., Curran, K., et al. (2017). Uncertainty in ocean-color estimates of chlorophyll for phytoplankton groups. *Frontiers in Marine Science*, *4*, 104. https://doi.org/10.3389/fmars.2017.00104

Brewin, R. J. W., Devred, E., Sathyendranath, S., Lavender, S. J., & Hardman-Mountford, N. J. (2011a). Model of phytoplankton absorption based on three size classes. *Applied Optics*, *50*(22), 4535–4549. https://doi.org/10.1364/AO.50.004535

Brewin, R. J. W., Hardman-Mountford, N. J., Lavender, S. J., Raitsos, D. E., Hirata, T., Uitz, J., et al. (2011b). An intercomparison of bio-optical techniques for detecting dominant phytoplankton size class from satellite remote sensing. *Remote Sensing of Environment*, *115*(2), 325–339. https://doi.org/10.1016/j.rse.2010.09.004

Brewin, R. J. W., Hirata, T., Hardman-Mountford, N. J., Lavender, S. J., Sathyendranath, S., & Barlow, R. (2012). The influence of the Indian Ocean Dipole on interannual variations in phytoplankton size structure as revealed by Earth Observation. *Deep Sea Research Part II: Topical Studies in Oceanography*, *77–80*, 117–127. https://doi.org/10.1016/j.dsr2.2012.04.009

Brewin, R. J. W., Sathyendranath, S., Hirata, T., Lavender, S. J., Barciela, R. M., & Hardman-Mountford, N. J. (2010). A three-component model of phytoplankton size class for the Atlantic Ocean. *Ecological Modeling*, *221*(11), 1472–1483. https://doi.org/10.1016/j.ecolmodel.2010.02.014

Brewin, R. J. W., Sathyendranath, S., Jackson, T., Barlow, R., Brotas, V., Airs, R., & Lamont, T. (2015). Influence of light in the mixed-layer on the parameters of a three-component model of phytoplankton size class. *Remote Sensing of Environment*, *168*, 437–450. https://doi.org/10.1016/j.rse.2015.07.004

Brewin, R. J. W., Sathyendranath, S., Tilstone, G., Lange, P. K., & Platt, T. (2014). A multicomponent model of phytoplankton size structure. *Journal of Geophysical Research: Oceans*, *119*, 3478–3496. https://doi.org/10.1002/2014JC009859

Brotas, V., Brewin, R. J. W., Sá, C., Brito, A. C., Silva, A., Mendes, C. R., et al. (2013). Deriving phytoplankton size classes from satellite data: Validation along a trophic gradient in the eastern Atlantic Ocean. *Remote Sensing of Environment*, *134*, 66–77. https://doi.org/10.1016/j.rse.2013.02.013

Cao, W., & Yang, Y. (2002). A bio-optical model for ocean photosynthetic available radiation. *Tropic Oceanology*, *21*(3), 47–54.

Cermeño, P., Marañón, E., Rodríguez, J., & Fernández, E. (2005). Large-sized phytoplankton sustain higher carbon- specific photosynthesis than smaller cells in a coastal eutrophic ecosystem. *Marine Ecology Progress Series*, *297*, 51–60. https://doi.org/10.3354/meps297051

Chen, C. T. A., Ruo, R., Paid, S. C., Liu, C. T., & Wong, G. T. F. (1995). Exchange of water masses between the East China Sea and the Kuroshio off northeastern Taiwan. *Continental Shelf Research*, *15*(1), 19–39. https://doi.org/10.1016/0278-4343(93)E0001-O

Chen, J., Huang, B., Liu, Y., Cao, Z., & Hong, H. (2006). Phytoplankton community structure in the transects across east China Sea and Northern South China sea determined by analysis of HPLC photosynthetic pigment signatures. *Advances in Earth Science*, *21*(7), 738–746.

Chisholm, S. W., Olson, R. J., Zettler, E. R., Goericke, R., Waterbury, J. B., & Welschmeyer, N. A. (1988). A novel free-living prochlorophyte abundant in the oceanic euphotic zone. *Nature*, *334*, 340–343. https://doi.org/10.1038/334340a0

Choi, J., Min, J., Noh, J. H., Han, T., Yoon, S., Park, Y. J., et al. (2014). Harmful algal bloom (HAB) in the East Sea identified by the Geostationary Ocean Color Imager (GOCI). *Harmful Algae*, *39*, 295–302. https://doi.org/10.1016/j.hal.2014.08.010

Ciotti, A. M., & Bricaud, A. (2006). Retrievals of a size parameter for phytoplankton and spectral light absorption by colored detrital matter from water-leaving radiances at SeaWiFS channels in a continental shelf region off Brazil. *Limnology and Oceanography: Methods*, *4*, 237–253. https://doi.org/10.4319/lom.2006.4.237

Ciotti, A. M., Lewis, M. R., & Cullen, J. J. (2002). Assessment of the relationships between dominant cell size in natural phytoplankton communities and the spectral shape of the absorption coefficient. *Limnology and Oceanography*, *47*(2), 404–417. https://doi.org/10.4319/lo.2002.47.2.0404

Cloern, J. E. (2001). Our evolving conceptual model of the coastal eutrophication problem. *Marine Ecology Progress Series*, *210*, 223–253. https://doi.org/10.3354/meps210223

Dai, X., Lu, D., Guan, W., Xia, P., Wang, H., He, P., et al. (2013). The Correlation between Prorocentrum donghaiense Blooms and the Taiwan Warm Current in the East China Sea - Evidence for the "Pelagic Seed Bank" Hypothesis. *Plos One*, *8*(5), e64188. https://doi.org/10.1371/journal.pone.0064188

Deng, C., Yu, Z., Yao, P., Chen, H., & Xue, C. (2008). Size-fractionated phytoplankton in the East China and Southern Yellow Seas and its environmental factors in autumn 2000. *Periodical of Ocean University of China*, *38*(5), 791–798

Devred, E., Sathyendranath, S., Stuart, V., Maass, H., Ulloa, O., & Platt, T. (2006). A two-component model of phytoplankton absorption in the open ocean: Theory and applications. *Journal of Geophysical Research*, *111*, C03011. https://doi.org/10.1029/2005JC002880

Devred, E., Sathyendranath, S., Stuart, V., & Platt, T. (2011). A three component classification of phytoplankton absorption spectra: Application to ocean-color data. *Remote Sensing of Environment*, *115*(9), 2255–2266. https://doi.org/10.1016/j.rse.2011.04.025

Dogliotti, A. I., Ruddick, K. G., Nechad, B., Doxaran, D., & Knaeps, E. (2015). A single algorithm to retrieve turbidity from remotely-sensed data in all coastal and estuarine waters. *Remote Sensing of Environment*, *156*, 157–168. https://doi.org/10.1016/j.rse.2014.09.020

Finkel, Z. V., Beardall, J., Flynn, K. J., Quigg, A., Rees, T. A. V., & Raven, J. A. (2010). Phytoplankton in a changing world: Cell size and elemental stoichiometry. *Journal of Plankton Research*, *32*(1), 119–137. https://doi.org/10.1093/plankt/fbp098

Finkel, Z. V., Irwin, A. J., & Schofield, O. (2004). Resource limitation alters the 3/4 size scaling of metabolic rates in phytoplankton. *Marine Ecology Progress*, *273*(1), 269–279. https://doi.org/10.3354/meps273269

Fu, M., Wang, Z., Li, Y., Li, R., Sun, P., Wei, X., et al. (2009). Phytoplankton biomass size structure and its regulation in the Southern Yellow Sea (China): Seasonal variability. *Continental Shelf Research*, *29*(18), 2178–2194. https://doi.org/10.1016/j.csr.2009.08.010

Gao, Y., Jiang, Z., Liu, J., Chen, Q., Zeng, J., & Huang, W. (2013). Seasonal variations of net-phytoplankton community structure in the southern Yellow Sea. *Journal of Ocean University of China*, *12*(4), 557–567. https://doi.org/10.1007/s11802-013-2258-x

Gao, Y., Yu, Q., Qi, Y., Zhou, J., Lu, D., Li, Y., et al. (2003). Species composition and ecological distribution of planktonic diatoms in the Changjiang River estuary during Spring. *The Chinese Journal of Applied Ecology*, *14*(7), 1044–1048.

Ge, J., Shen, F., Guo, W., Chen, C., & Ding, P. (2015). Estimation of critical shear stress for erosion in the Changjiang Estuary: A synergy research of observation, GOCI sensing and modeling. *Journal of Geophysical Research: Oceans*, *120*, 8439–8465. https://doi.org/10.1002/2015JC010992

Geider, R. J., MacIntyre, H. L., & Kana, T. M. (1998). A dynamic regulatory model of phytoplanktonic acclimation to light, nutrients, and temperature. *Limnology and Oceanography*, *43*(4), 679–694. https://doi.org/10.4319/lo.1998.43.4.0679

Geider, R. J., Platt, T., & Raven, J. A. (1986). Size dependence of growth and photosynthesis in diatoms: A synthesis. *Marine Ecology Progress*, *30*(1), 93–104

Gong, G. C., Wen, Y. H., Wang, B. W., & Liu, G. J. (2003). Seasonal variation of chlorophyll a concentration, primary production and environmental conditions in the subtropical East China Sea. *Deep Sea Res., Part II: Topical Studies in Oceanography*, *50*(6–7), 1219–1236. https://doi.org/10.1016/S0967-0645(03)00019-5

Guo, S., Feng, Y., Wang, L., Dai, M., Liu, Z., Bai, Y., et al. (2014). Seasonal variation in the phytoplankton community of a continental-shelf sea: The East China Sea. *Marine Ecology Progress Series*, *516*, 103–126. https://doi.org/10.3354/meps10952

He, X., Bai, Y., Pan, D., Huang, N., Dong, X., Chen, J., et al. (2013). Using geostationary satellite ocean color data to map the diurnal dynamics of suspended particulate matter in coastal waters. *Remote Sensing of Environment*, *133*, 225–239. https://doi.org/10.1016/j.rse.2013.01.023

Hilligsøe, K., Richardson, K., Bendtsen, J., Sorensen, L., Nielsen, T., & Lyngsgaard, M. (2011). Linking phytoplankton community size composition with temperature, plankton food web structure and sea–air CO2 flux. *Deep Sea Res., Part I: Oceanographic Research Papers*, *58*(8), 826–838. https://doi.org/10.1016/j.dsr.2011.06.004

Hirata, T., Hardman-Mountford, N. J., Barlow, R., Lamont, T., Brewin, R., Smyth, T., et al. (2009). An inherent optical property approach to the estimation of size-specific photosynthetic rates in eastern boundary upwelling zones from satellite ocean colour: An initial assessment. *Progress in Oceanography*, *83*(1–4), 393–397. https://doi.org/10.1016/j.pocean.2009.07.019

Hirata, T., Hardman-Mountford, N. J., Brewin, R. J. W., Aiken, J., Barlow, R., Suzuki, K., et al. (2011). Synoptic relationships between surface Chlorophyll-a and diagnostic pigments specific to phytoplankton functional types. *Biogeosciences*, *8*(2), 311–327. https://doi.org/10.5194/bg-8-311-2011

Hu, Z., Pan, D., He, X., & Bai, Y. (2016a). Diurnal variability of turbidity fronts observed by geostationary satellite ocean color remote sensing. *Remote Sensing*, *8*(2), 147. https://doi.org/10.3390/rs8020147

Hu, Z., Wang, D., Pan, D., He, X., Miyazawa, Y., Bai, Y., et al. (2016b). Mapping surface tidal currents and Changjiang plume in the East China Sea from geostationary ocean color imager. *Journal of Geophysical Research: Oceans*, *121*, 1563–1572. https://doi.org/10.1002/2015JC011469

Huang, B., Liu, Y., Chen, J., Wang, D., Hong, H., Lu, R., et al. (2006). Temporal and spatial distribution of size-fractionized phytoplankton biomass in East China Sea and Huanghai Sea. *Acta Oceanologica Sinica*, *28*(2), 156–164.

IOCCG (2014). Phytoplankton functional types from space. In S. Sathyendranath (Ed.), *Reports of the international ocean-colour coordinating group* (15), Dartmouth, Canada: IOCCG.

Jephson, T., & Carlsson, P. (2009). Species and stratification-dependent diel vertical migration behaviour of three dinoflagellate species in a laboratory study. *Journal of Plankton Research*, *31*(11), 1353–1362. https://doi.org/10.1093/plankt/fbp078

Kostadinov, T. S., Siegel, D. A., & Maritorena, S. (2009). Retrieval of the particle size distribution from satellite ocean color observations. *Journal of Geophysical Research*, *114*, C09015. https://doi.org/10.1029/2009JC005303

Lee, Z., Jiang, M., Davis, C., Pahlevan, N., Ahn, Y., & Ma, R. (2012). Impact of multiple satellite ocean color samplings in a day on assessing phytoplankton dynamics. *Ocean Science Journal*, *47*(3), 323–329. https://doi.org/10.1007/s12601-012-0031-5

Legendre, L., & Rassoulzadegan, F. (1995). Plankton and nutrient dynamics in marine waters. *Ophelia*, *41*, 153–172. https://doi.org/10.1080/00785236.1995.10422042

Li, G., Han, X., Yue, S., Wen, G., Rongmin, Y., & Kusky, T. M. (2006). Monthly variations of water masses in the East China Seas. *Continental Shelf Research*, *26*(16), 1954–1970. https://doi.org/10.1016/j.csr.2006.06.008

Li, G., Qiao, L., Dong, P., Ma, Y., Xu, J., Liu, S., et al. (2016). Hydrodynamic condition and suspended sediment diffusion in the Yellow Sea and East China Sea. *Journal of Geophysical Research: Oceans*, *121*, 6204–6222. https://doi.org/10.1002/2015JC011442

Lie, H. J., Cho, C. H., Lee, J. H., Lee, S., & Tang, Y. (2001). Does the Yellow Sea Warm Current really exist as a persistent mean flow?. *Journal of Geophysical Research*, *106*(C10), 22199–22210. https://doi.org/10.1029/2000JC000629

Lindemann, C., & St. John, M. A. (2014). A seasonal diary of phytoplankton in the North Atlantic. *Frontiers in Marine Science*, *1*(37), 1–6. https://doi.org/10.3389/fmars.2014.00037

Lin, J., Cao, W., Wang, G., & Hu, S. (2014). Satellite-observed variability of phytoplankton size classes associated with a cold eddy in the South China Sea. *Marine Pollution Bulletin*, *83*(1), 190–197. https://doi.org/10.1016/j.marpolbul.2014.03.052

Liu, R., Zhang, J., Yao, H., Cui, T., Wang, N., Zhang, Y., et al. (2017). Hourly changes in sea surface salinity in coastal waters recorded by Geostationary Ocean Color Imager. *Estuarine, Coastal and Shelf Science*, *196*, 227–236. https://doi.org/10.1016/j.ecss.2017.07.004

Liu, X., Huang, B., Huang, Q., Wang, L., Ni, X., Tang, Q., et al. (2015). Seasonal phytoplankton response to physical processes in the southern Yellow Sea. *Journal of Sea Research*, *95*, 45–55. https://doi.org/10.1016/j.seares.2014.10.017

Loisel, H., Nicolas, J., Sciandra, A., Stramski, D., & Poteau, A. (2006). Spectral dependency of optical backscattering by marine particles from satellite remote sensing of the global ocean. *Journal of Geophysical Research*, *111*, C09024. https://doi.org/10.1029/2005JC003367

Lorenzen, C. J. (1963). Diurnal variation in photosynthetic activity of natural phytoplankton populations. *Limnology and Oceanography*, *8*(1), 56–62. https://doi.org/10.4319/lo.1963.8.1.0056

Lou, X., & Hu, C. (2014). Diurnal changes of a harmful algal bloom in the East China Sea: Observations from GOCI. *Remote Sensing of Environment*, *140*, 562–572. https://doi.org/10.1016/j.rse.2013.09.031

Madariaga, I., & Orive, E. (1989). Spatiotemporal variations of size- fractionated primary production in the Gernika estuary. *Journal of Experimental Marine Biology and Ecology*, *127*(3), 273–288. https://doi.org/10.1016/0022-0981(89)90079-8

Marañón, E. (2015). Cell size as a key determinant of phytoplankton metabolism and community structure. *Annual Review of Marine Science*, *7*, 241–264. https://doi.org/10.1146/annurev-marine-010814-015955

Marañón, E., Cermeño, P., López-Sandoval, D. C., Rodríguez-Ramos, T., Sobrino, C., Huete-Ortega, M., et al. (2013). Unimodal size scaling of phytoplankton growth and the size dependence of nutrient uptake and use. *Ecological Letters*, *16*(3), 371–379. https://doi.org/10.1111/ele.12052

Marañón, E., Holligan, P. M., Barciela, R., Gonzalez, N., Mourino, B., Pazo, M. J., et al. (2001). Patterns of phytoplankton size structure and productivity in contrasting open-ocean environments. *Marine Ecology Progress Series*, *216*, 43–56. https://doi.org/10.3354/meps216043

Maulood, B. K., Hinton, G. C. F., & Boney, A. D. (1978). Diurnal variation of phytoplankton in Loch Lomond. *Hydrobiologia*, *58*(2), 99–117. https://doi.org/10.1007/BF00007992

Mitbavkar, S., & Saino, T. (2015). Diurnal variability of Synechococcus abundance in Sagami Bay, Japan. *Hydrobiologia*, *747*(1), 133–145. https://doi.org/10.1007/s10750-014-2125-9

Nair, A., Sathyendranath, S., Platt, T., Morales, J., Stuart, V., Forget, M., et al. (2008). Remote sensing of phytoplankton functional types. *Remote Sensing of Environment*, *112*(8), 3366–3375. https://doi.org/10.1016/j.rse.2008.01.021

O'Reilly, J. E., Maritorena, S., Mitchell, B. G., Siegel, D. A., Carder, K. L., Garver, S. A., et al. (1998). Ocean color chlorophyll algorithms for SeaWiFS. *Journal of Geophysical Research*, *103*(C11), 24924–24937. https://doi.org/10.1029/98JC02160

Pan, Y., Shen, F., & Wei, X. (2018). Fusion of Landsat-8/OLI and GOCI Data for hourly mapping of suspended particulate matter at high spatial resolution: A case study in the Yangtze (Changjiang) estuary. *Remote Sensing*, *10*(2), 158. https://doi.org/10.3390/rs10020158

Quan, Q., Mao, X., Yang, X., Hu, Y., Zhang, H., & Jiang, W. (2013). Seasonal variations of several main water masses in the southern Yellow Sea and East China Sea in 2011. *Journal of Ocean University of China*, *12*(4), 524–536. https://doi.org/10.1007/s11802-013-2198-5

Ras, J., Claustre, H., & Uitz, J. (2007). Spatial variability of phytoplankton pigment distributions in the Subtropical South Pacific Ocean: Comparison between in situ and predicted data. *Biogeosciences*, *5*(2), 353–369. https://doi.org/10.5194/bg-5-353-2008

Ryu, J. H., Choi, J. K., Eom, J., & Ahn, J. H. (2011). Temporal variation in Korean coastal waters using geostationary ocean color imager. *Journal of Coastal Research*, *SI64*, 1731–1735

Sathyendranath, S., Cota, G., Stuart, V., Maass, H., & Platt, T. (2001). Remote sensing of phytoplankton pigments: A comparison of empirical and theoretical approaches. *International Journal of Remote Sensing*, *22*(2), 249–273. https://doi.org/10.1080/014311601449925

Sieburth, J. M., Smetacek, V., & Lenz, J. (1978). Pelagic ecosystem structure: Heterotrophic compartments of the plankton and their relationship to plankton size fractions. *Limnology and Oceanography*, *23*(6), 1256–1263. https://doi.org/10.4319/lo.1978.23.6.1256

Siswanto, E., Tang, J., Yamaguchi, H., Ahn, Y., Ishizaka, J., Yoo, S., et al. (2011). Empirical ocean-color algorithms to retrieve chlorophyll-a, total suspended matter, and colored dissolved organic matter absorption coefficient in the Yellow and East China Seas. *Journal of Oceanography*, *67*(5), 627–650. https://doi.org/10.1007/s10872-011-0062-z

Song, S., Li, Z., Li, C., & Yu, Z. (2017). The response of spring phytoplankton assemblage to diluted water and upwelling in the eutrophic Changjiang (Yangtze River) Estuary. *Acta Oceanologica Sinica*, *36*(12), 101–110. https://doi.org/10.1007/s13131-017-1094-z

Sun, D., Huan, Y., Qiu, Z., Hu, C., Wang, S., & He, Y. (2017). Remote-sensing estimation of phytoplankton size classes from GOCI satellite measurements in Bohai Sea and Yellow Sea. *Journal of Geophysical Research: Oceans*, *122*, 8309–8325. https://doi.org/10.1002/2017JC013099

Sun, J., Liu, D., Yang, S., Guo, J., & Qian, S. (2002). The preliminary study on phytoplankton community structure in the central Bohai sea and the Bohai strait and its adjacent area. *Oceanologia et Limnologia Sinica*, *33*(5), 461–471.

Sun, X., Dong, S., & Tang, Z. (2008). Influences of nutrients and illuminance on phytoplankton community structure. *South China Fisheries Science*, *4*(1), 1–9.

Sun, X., Ren, L., Zheng, S., Wen, F., Zhao, Y., & Sun, S. (2012). Phytoplankton size structure in the yellow sea and East China Sea in the spring and summer of 2011. *Oceanologia et Limnologia Sinica*, *43*(3), 419–428.

Tassan, S. (1994). Local algorithms using SeaWiFS data for the retrieval of phytoplankton, pigments, suspended sediment, and yellow substance in coastal waters. *Applied Optics*, *33*(12), 2369–2378. https://doi.org/10.1364/AO.33.002369

Teira, E., Serret, P., & Fernandez, E. (2001). Phytoplankton size-structure, particulate and dissolved organic carbon production and oxygen fluxes through microbial communities in the NW Iberian coastal transition zone. *Marine Ecology Progress Series*, *219*, 65–83. https://doi.org/10.3354/meps219065

Uitz, J., Claustre, H., Morel, A., & Hooker, S. B. (2006). Vertical distribution of phytoplankton communities in open ocean: An assessment based on surface chlorophyll. *Journal of Geophysical Research*, *111*, C08005. https://doi.org/10.1029/2005JC003207

Uitz, J., Huot, Y., Bruyant, F., Babin, M., & Claustre, H. (2008). Relating phytoplankton photophysiological properties to community structure on large scale. *Limnology and Oceanography*, *53*(2), 614–630. https://doi.org/10.4319/lo.2008.53.2.0614

Vaulot, D., & Marie, D. (1999). Diel variability of photosynthetic picoplankton in the equatorial Pacific. *Journal of Geophysical Research*, *104*(C2), 3297–3310. https://doi.org/10.1029/98JC01333

Vidussi, F., Claustre, H., Manca, B., Luchetta, A., & Marty, J. (2001). Phytoplankton pigment distribution in relation to upper thermocline circulation in the eastern Mediterranean Sea during winter. *Journal of Geophysical Research*, *106*(C9), 19939–19956. https://doi.org/10.1029/1999JC000308

Waite, A. M., Fisher, A., Thompson, P. A., & Harrison, P. J. (1997). Sinking rate versus volume relationships illuminate sinking control mechanisms in marine diatoms. *Marine Ecology Progress Series*, *157*(8), 97–108

Wang, B., Wang, X., & Zhan, R. (2003). Nutrient conditions in the Yellow Sea and the East China Sea. *Estuarine, Coastal and Shelf Science*, *58*(1), 127–136. https://doi.org/10.1016/S0272-7714(03)00067-2

Wang, L., Huang, B., Chiang, K., Liu, X., Chen, B., Xie, Y., et al. (2016). Physical-biological coupling in the Western South China Sea: The response of phytoplankton community to a mesoscale cyclonic eddy. *Plos One*, *11*(4), e153735. https://doi.org/10.1371/journal.pone.0153735

Ward, B. A., Dutkiewicz, S., Jahn, O., & Follows, M. J. (2012). A size-structured food-web model for the global ocean. *Limnology and Oceanography*, *57*(6), 1877–1891. https://doi.org/10.4319/lo.2012.57.6.1877

Xia, P., Lu, D., Zhu, D., & Du, W. (2007). Trend and characteristics of harmful algal blooms in Zhejiang coastal waters. *Journal of Marine Sciences*, *25*(02), 47–56.

Yentsch, C. S., & Phinney, D. A. (1989). A bridge between ocean optics and microbial ecology. *Limnology and Oceanography*, *34*(8), 1694–1705. https://doi.org/10.4319/lo.1989.34.8.1694

Yu, F., Zhang, Z., Lan, J., Diao, X., Guo, J., & Ge, R. (2005). Analysis of Water Temperature Distribution Characteristics in the Southern Yellow Sea in Spring. *Advances in Marine Science*, *23*(3), 281–288.

Zhang, J., Liu, D., Cao, P., Wang, Y., Keesing, J. K., Li, J., & Chen, L. (2016). A highly sensitive method for analyzing marker phytoplankton pigments: Ultra-high-performance liquid chromatography-tandem triple quadrupole mass spectrometry. *Limnology and Oceanography: Methods*, *14*(10), 623–636. https://doi.org/10.1002/lom3.10117

Zhang, J., Liu, S. M., Ren, J. L., Wu, Y., & Zhang, G. L. (2007). Nutrient gradients from the eutrophic Changjiang (Yangtze River) Estuary to the oligotrophic Kuroshio waters and re-evaluation of budgets for the East China Sea Shelf. *Progress in Oceanography*, *74*(4), 449–478. https://doi.org/10.1016/j.pocean.2007.04.019

Zhang, S. W., Wang, Q. Y., Lü, Y., Cui, H., & Yuan, Y. L. (2008). Observation of the seasonal evolution of the Yellow Sea Cold Water Mass in 1996–1998. *Continental Shelf Research*, *28*(3), 442–457. https://doi.org/10.1016/j.csr.2007.10.002

Zhou, M., Yan, T., & Zou, J. (2003). Preliminary analysis of the characteristics of red tide areas in Changjiang River estuary and its adjacent sea. *Chinese Journal of Applied Ecology*, *14*(7), 1031–1038.

Zhu, Z., Ng, W., Liu, S., Zhang, J., Chen, J., & Wu, Y. (2009). Estuarine phytoplankton dynamics and shift of limiting factors: A study in the Changjiang (Yangtze River) Estuary and adjacent area. *Estuarine, Coastal and Shelf Science*, *84*(3), 393–401. https://doi.org/10.1016/j.ecss.2009.07.005